



On the Configuration and Initialization of a Large Scale Hydrological Land Surface Model to Represent Permafrost

1 Mohamed E. Elshamy^{1*}, Daniel Princz², Gonzalo Sapriza-Azuri³, Al Pietroniro^{1,2}, Howard S. Wheeler¹, and
2 Saman Razavi¹

3 ¹ Global Institute for Water Security, University of Saskatchewan, 11 Innovation Blvd, Saskatoon, SK,
4 Canada S7N 3H5

5 ² Environment and Climate Change Canada, 11 Innovation Blvd, Saskatoon, SK, Canada S7N 3H5

6 ³ Departamento del Agua, Centro Universitario Regional Litoral Norte, Universidad de la República, Salto,
7 Uruguay

8 ***Corresponding author:** mohamed.elshamy@usask.ca

Abstract

9 Permafrost is an important feature of cold regions hydrology, particularly in basins such as the Mackenzie
10 River Basin (MRB), and needs to be properly represented in hydrological and land surface models (H-LSMs)
11 built into existing Earth System models (ESM), especially under the unprecedented climate warming
12 trends that have been observed. Higher rates of warming have been reported in high latitudes compared
13 to the global average resulting in permafrost thaw with wide-ranging implications for hydrology and
14 feedbacks to climate. The current generation of H-LSMs is being improved to simulate permafrost
15 dynamics by allowing deep soil profiles and incorporating organic soils explicitly. Deeper soil profiles have
16 larger hydraulic and thermal memories that require more effort to initialize. This study aims to devise a
17 robust, yet computationally efficient, initialization and parameterization approach applicable to regions
18 where data are scarce and simulations typically require large computational resources. The study further
19 demonstrates an upscaling approach to inform large-scale ESM simulations based on the insights gained
20 by modelling at small scales. We used permafrost observations from three sites along the Mackenzie River
21 Valley spanning different permafrost classes to test the validity of the approach. Results show generally
22 good performance in reproducing present-climate permafrost properties at the three sites. The results
23 also emphasize the sensitivity of the simulations to the soil layering scheme used, the depth to bedrock
24 and the organic soil properties.

Keywords

25 Hydrological Land Surface Models, Permafrost, Initialization, Organic Soils, Mackenzie River Basin



1. Introduction

26 Earth system models (ESMs) are widely used to project climate change and they show a current global
27 warming trend that is expected to continue during the 21st century and beyond (IPCC, 2014). Higher rates
28 of warming have been observed in high latitudes compared to the global average (DeBeer et al., 2016;
29 McBean et al., 2005) resulting in permafrost thaw with implications for soil moisture, hydraulic
30 connectivity, streamflow seasonality, land subsidence, and vegetation (Walvoord and Kurylyk, 2016).
31 Recent analyses provided by Environment and Climate Change Canada (Zhang et al., 2018) have shown
32 that Canada's far north has already seen an increase in temperature of double the global average, with
33 some portion of the Mackenzie basin already heating up by 4°C. Subsequent impacts on water resources
34 in the region however, are not so clear. Recent analysis of trends in Arctic freshwater inputs (Durocher
35 et al., 2019) highlights that Eurasian rivers show a significant annual discharge increase during 1975-2015
36 period while in North American rivers; only rivers flowing into the Hudson Bay region in Canada show a
37 significant annual discharge change during that same period. Those rivers in Canada flowing directly into
38 the Arctic, of which the Mackenzie River provides the majority of flow, show very little change.

39 Deep uncertainty in hydrological response to a changing climate is resulting from poor understanding and
40 characterization of cold-regions processes in ESMs. Despite advances in cold-regions process
41 understanding and modelling at the local scale (e.g. Pomeroy et al., 2007), their upscaling and systematic
42 evaluation over large domains remain rather elusive. This is largely due to lack of observational data, the
43 local nature of these phenomena and the complexity of cold-region systems. Hydrological response and
44 land-surface feedbacks in cold-regions are generally complex and depend on a multitude of several inter-
45 related factors including changes to precipitation intensity, timing, and phase as well as soil composition
46 and hydraulic and thermal properties. As permafrost underlies about one quarter of the exposed land in
47 the Northern hemisphere (Zhang et al., 2008), it is imperative to study and accurately model its behaviour
48 under current and future climate conditions. Knowledge of permafrost conditions (temperature, active
49 layer thickness, and ground ice conditions) and their spatial and temporal variations is critical for planning
50 of development in Northern Canada (Smith et al., 2007) and other Arctic environments.

51 There has been extensive regional and global modelling efforts which involve cold-region processes
52 including permafrost (Riseborough et al., 2008; Walvoord and Kurylyk, 2016). These studies, however,
53 typically focused on and modeled only a shallow soil profile in the order of a few meters. For example,
54 the Canadian Land Surface Scheme (CLASS) typically uses 4.1m (Versegny, 2012) and the Joint UK Land
55 Environment Simulator (JULES) standard configuration is only 3.0m (Best et al., 2011). These are too



56 shallow to represent permafrost properly and could result in misleading projections. For example,
57 Lawrence and Slater (2005) used a 3.43m soil column to project the impacts of climate change on near-
58 surface permafrost degradation in the Northern hemisphere using the Community Climate System Model
59 (CCSM3), which lead to overestimation of climate change impacts and raised considerable criticism (e.g.
60 Burn and Nelson, 2006). It eventually lead to further development of the Community Land Model (CLM),
61 the land surface scheme of the CCSM, to include deeper soil profiles (e.g. Swenson et al., 2012).
62 Recognizing this issue, more recent studies have indicated the need to have a deeper soil column (20-25m
63 at least) in land surface models (run stand-alone or embedded within ESMs) than previously used, to
64 properly capture changes in freeze and thaw cycles and active layer depth dynamics (Lawrence et al.,
65 2012; Romanovsky and Osterkamp, 1995; Sapriza-Azuri et al., 2018).

66 However, a deeper soil column implies larger soil hydraulic and, more importantly, thermal memory that
67 requires proper initialization to be able to capture the evolution of past, current and future changes. Initial
68 conditions are established by either spinning up the model for many annual cycles (or multi-year historical
69 cycles, sometimes de-trended) to reach some steady state or by running it for a long transient simulation
70 for 100s of years or both (spinning to stabilization followed by a long transient simulation). Lawrence et
71 al. (2008) spun up CLM3.5 for 400 cycles with year 1900 data for deep soil profiles (50-125m) to assess
72 the sensitivity of model projections to soil column depth and organic soil representation. Park et al. (2013)
73 used 21 cycles of the first 20 years of the climate record they used (1948-2006) to initialize their CHANGE
74 land surface model to study differences in active layer thickness between Eurasian and North American
75 watersheds. However, Ednie et al. (2008) implied from borehole observations in the Mackenzie Valley
76 that present day permafrost is in disequilibrium with current climate, and therefore, it is unlikely that we
77 can establish a reasonable representation of current ground thermal conditions by employing present or
78 20th century climate conditions to start the simulations. Nevertheless, their analysis of paleo-climatic
79 records (Szeicz and MacDonald, 1995) of summer temperature at Fort Simpson, dating back to the early
80 1700s, shows that a negative (cooling) trend prevailed till mid 1800s followed by a positive (warming)
81 trend till present and they “assumed” a quasi-equilibrium period prior to 1720. Using that assumption,
82 they used an equilibrium thermal model called T-TOP to establish the initial conditions of 1721 and then
83 the temperature trends thereafter to carry out a transient simulation till 2000 using the T-ONE thermal
84 model. Those thermal models use air temperature as their main input while land surface models (as used
85 here and described below) require a suite of meteorological inputs. Sapriza-Azuri et al. (2018) used tree-
86 ring data from Szeicz and Macdonald (1995) to construct climate records for all variables required by
87 CLASS at Norman Wells in the Mackenzie Valley since 1638 to initialize the soil profile of their model.



88 While useful, such proxy records are not easily available at most sites. Additionally, re-constructing several
89 climatic variables from summer temperature introduces significant uncertainties that need to be
90 assessed. Thus, there is a need to formulate a more generic way to define the initial conditions of soil
91 profiles across large domains.

92 Additionally, concerns are not only about the depth of the whole profile. The definition of the layer
93 thicknesses requires due attention. Land surface models that utilize deep soil profiles exponentially
94 increase the layer thicknesses to reach the total depth using a reasonably tractable number of layers (15-
95 20). For example, CLM 4.5 (Oleson et al., 2013) used 15 layers to reach a depth of 42.1m for the soil
96 column. Sapriza-Azuri et al. (2018) used 20 layers to reach a depth of 71.6m in their experiments using
97 MESH/CLASS. Park et al. (2013) had a 15-layer soil column with exponentially increasing depth to reach a
98 total depth of 30.5m in the CHANGE land surface model. However, the first version of CHANGE had only
99 11m soil column depth (Park et al., 2011).

100 The importance of insulation from the snow cover on the ground and/or organic matter in the upper soil
101 layers is key to the quality of ALD simulation results (Lawrence et al., 2008; Park et al., 2013). Organic soils
102 have large heat and moisture capacities that, depending on their depth and composition, moderate the
103 effects of the atmosphere on the deeper permafrost layers and work all year round. Snow cover, in
104 contrast, varies seasonally and inter-annually and can thus induce large variations to the ALD, especially
105 in the absence of organic matter (Park et al., 2011). Climate change impacts on precipitation intensity,
106 timing, and phase are translated to permafrost impacts via changing the snow cover period, spatial extent,
107 and depth. Therefore, it is critical to the simulation of ALD that the model includes organic soils and has
108 adequate representation of snow accumulation (including sublimation and transport) and melt processes.

2. Objectives

109 The main objective of the present study is to devise an approach to configure and initialize the soil profile
110 of a land surface model to account for permafrost in large-scale applications. The elements of this strategy
111 include:

- 112 - Defining how deep should the soil profile be, to allow proper simulation of the ALD dynamics for
113 current and future climate.
- 114 - Determining the appropriate vertical discretization to give enough accuracy in determining the
115 ALD while optimizing computational resources for large-scale applications. This also includes



116 configuring the organic layers (how many, which properties, etc.) and the depth to bedrock (see
117 description below).

118 - Determining how to initialize the deep soil profile, whether cycling a single year or multiple years
119 and finding the appropriate number of cycles. In addition to studying the sensitivity of
120 performance to the selected year(s) for spinning.

121 This study is part of a larger study that aims to develop a large-scale hydrological model for the Mackenzie
122 River Basin (MRB) (Figure 1) using the MESH (Modélisation Environnementale Communautaire - Surface and
123 Hydrology) framework and validate the model in order to use it to study climate and land use/cover
124 change impacts on various aspects of its hydrology. Permafrost underlies 70-80% of the MRB and thus it
125 exerts considerable control on its hydrology, especially in a warming climate. The next section describes
126 the model briefly and the datasets and methods used in the study. Section 4 displays the results of the
127 analyses that are discussed in Section 5 with some concluding remarks.

128 **Possible position for Figure 1**

3. Models, Methods, and Datasets

3.1 The MESH Modelling Framework

129 MESH is a semi-distributed hydrological-land surface model (H-LSM) coupled with streamflow routing
130 (Pietroniro et al., 2007). It has been widely used in Canada to study the Great Lakes Basin (Haghnegahdar
131 et al., 2015) and the Saskatchewan River Basin (Yassin et al., 2017) amongst others. Several applications
132 to basins outside Canada are underway (e.g. Arboleda-Obando, 2018; Bahremand et al., 2018). The MESH
133 framework allows coupling of a land surface model, either CLASS (Verseghy, 2012) or SVS (Husain et al.,
134 2016) that models the vertical processes of heat and moisture flux transfers between the land surface and
135 the atmosphere, with a horizontal routing component (WATROUTE) taken from the distributed
136 hydrological model WATFLOOD (Kouwen, 1988). Unlike most land surface models, the vertical column has
137 a slope that allows for lateral transfer of overland and interflow (Soulis et al., 2000) to an assumed stream
138 within each grid cell of the model. MESH uses a regular latitude-longitude grid and represents subgrid
139 heterogeneity using the grouped response unit (GRU) approach (Kouwen et al., 1993) which makes it
140 semi-distributed. In the GRU approach, different land covers within a grid cell do not have specific
141 locations and do not interact explicitly, making it easier for parameterization. While, Land cover classes
142 are typically used to define a GRU, other factors can be included in the definition such as soil type, slope,
143 aspect, etc. A tile, which is the smallest computational element, is defined by a specific GRU in a given grid



144 cell. MESH has been under continuous development; its new features include improved representation of
145 baseflow (Luo et al., 2012), controlled reservoirs (Yassin et al., 2019) as well as permafrost (this paper).
146 More details about MESH history and developments are provided in a companion paper (Davison et al.,
147 in preparation). For this study, we use CLASS as the underlying land surface model within MESH.

148 Underground, CLASS couples the moisture and energy balances for a pre-specified number of soil layers
149 of pre-specified thicknesses. Each soil layer, thus, has a diagnosed temperature and both liquid and frozen
150 moisture contents down to the soil permeable depth or the “depth to bedrock – SDEP” below which there
151 is no moisture and the thermal properties of the soil are assumed as those of bedrock material
152 (sandstone). MESH is usually run at 30min time steps and thus from the MESH-simulated continuous
153 temperature profiles, one can determine several permafrost related aspects that are used in the analyses
154 such as (see Figure 2):

- 155 - Temperature envelopes at daily, monthly and annual time steps. Temperature envelopes are
156 defined by the maximum and minimum simulated temperature for each layer over the specified
157 time period.
- 158 - Active layer thickness (or depth – ALD) defined as the maximum depth of the zero isotherm over
159 the year taken from the annual temperature envelopes by linear interpolation between layers
160 bracketing the zero value (freezing point depression is not considered). It has to be connected to
161 the surface, thus we use a thaw, rather than freeze, criterion, which is compatible with the
162 available measurements.
- 163 - Daily progression of the ALD, which can be used to visualize the thaw and freeze fronts and
164 determine the dates of thaw and freeze-up. These are calculated in a similar way to the annual
165 ALD but using the daily envelopes.
- 166 - The no (or zero) oscillation depth (ZOD) where the annual temperature envelopes meet to within
167 0.1° (or other given accuracy threshold). In some literature, this depth is termed the zero
168 amplitude depth (ZA).

169

Possible position for see Figure 2

170 Permafrost is usually defined as ground remaining frozen for at least two years but for modelling purposes
171 and to validate against annual ground temperature envelope and ALD data, a one-year cycle is adopted.
172 This is common amongst the climate and land surface modelling community (e.g. Park et al., 2013).
173 MESH/CLASS used to output temperature profiles; the code has been amended to calculate the additional
174 outputs detailed above for each tile as well as the grid average allowing spatial and temporal mapping of



175 permafrost characteristics. A CLASS typical configuration consists of 3 soil layers of 0.1, 0.25, and 3.75m
176 thickness but in 2006, it was extended to accommodate as many layers as needed (Verseghy, 2012).
177 However, this was hard-coded within CLASS until it became configurable using an external file only within
178 the MESH framework. The configuration file used to provide soil parameters (texture and initial
179 temperature and moisture conditions) for each GRU for the top three layers and the model assumed the
180 third layer values to apply to any additional layers below till bedrock. The code has been modified to
181 enable specifying these parameters for as many layers as needed and was extended to allow a spatially
182 variable specification (i.e. by grid) of these parameters as well as by GRU. However, the number and
183 thickness of soil layers are still fixed for the whole domain.

184 Organic soils are modelled in CLASS by deactivating mineral soils using a special flag to allow a soil layer
185 to either be Fibric, Hemic, or Sapric after Letts et al. (2000). Each type has a different degree of
186 decomposition leading to different physical, hydraulic and thermal properties as specified in Verseghy
187 (2012). Usually, a soil layer is assumed to be fully organic if the organic content is 30% or more (Soil
188 Classification Working Group, 1998). Organic soils were mapped from the Soil Landscapes of Canada (SLC)
189 v2.2 (Centre for Land and Biological Resources Research, 1996) for the whole MRB (Figure 3). However,
190 this dataset does not provide information as to the depth of the organic layers or their configuration (i.e.
191 the thicknesses of Fibric, Hemic and Sapric layers). Therefore, different configurations have been tested
192 at the study sites based on available local information keeping in mind that these has to be carried back
193 to the MRB scale.

194

Possible Position for Figure 3

3.2 Study Sites and Data

195 The Mackenzie River Basin (MRB) extends between 102-140°W and 52-69°N (Figure 1). It drains an area
196 of about 1.775 Mkm² of Western and Northwestern Canada and covers parts of Saskatchewan, Alberta,
197 British Columbia provinces as well as the Yukon and the North West Territories. The average annual
198 discharge at the basin outlet to the Beaufort Sea exceeds 300 km³, which is the fifth largest discharge to
199 the Arctic. Such a large discharge influences regional as well as global circulation patterns under the
200 current climate, and is expected to have implications for climate change. Figure 1 also shows the
201 permafrost extent and categories for the MRB taken from the Canadian Permafrost Map (Hegginbottom
202 et al., 1995). About 75% of the basin is underlain by permafrost that can be either continuous (in the far
203 North and the Western Mountains), discontinuous (to the south of the continuous region), or sporadic (in
204 the southern parts of the Liard and in the Hay sub-basin). It is important, while building the MRB model,



205 to properly represent permafrost, given the current trends of thawing and its vast impacts on landforms,
206 connectivity, and thus the hydrology of the basin. This is the focus of this paper, through detailed studies
207 conducted at three sites on a transect near the Mackenzie River going from the Sporadic permafrost zone
208 (Jean Marie River) to the Extensive Discontinuous zone (Norman Wells) and the Extensive Continuous
209 zone (Havikpak Creek) as shown Figure 1. The following sections give a closer look at each site, the data
210 available, and some of the previous work conducted, focusing on permafrost.

211 3.2.1 Jean Marie River

212 The Jean Marie River (JMR) is a tributary of the main Mackenzie River Basin (Figure 4) in the Northwest
213 Territories (NWT) province of Canada. Its mouth is located upstream of Fort Simpson where the Liard River
214 joins the main Mackenzie River. The gauged area up to the WSC station at the river intersection with
215 Highway 1 is about 1240 km². The basin is dominated by boreal (deciduous, coniferous and mixed) forest
216 on raised peat plateaux and bogs. The basin is located in the sporadic permafrost zone characterized with
217 warm permafrost (temperature > -1°C) that underlies some parts and does not exist in others with limited
218 (<10m) thickness (Smith and Burgess, 2002).

219 Possible Position for Figure 4

220 The nearest Environment and Climate Change Canada (ECCC) Weather station is located at Fort Simpson
221 to the North of the Basin. The Canadian Climate Normals (1981–2010, ECCC) at Fort Simpson indicates
222 that the mean annual temperature is -2.8°C with temperatures generally below freezing during October
223 to April while a maximum summer temperature of 17.4°C is reached in July. Mean annual precipitation is
224 about 388 mm/year, of which around 60% falls as rain while the rest is snowfall.

225 The streamflow at Water Survey of Canada (WSC) gauge 10FB005 has a good record for the period 1972-
226 2015. The basin is snow-melt dominated with flow peaks normally occurring in May/June with some years
227 having secondary summer peaks. The mean annual streamflow at the station over the period 1980-2015
228 is 5.5 m³/s, while the highest recorded streamflow reached 211 m³/s on July 3, 1988. Baseflow is usually
229 small but the river does not run completely dry in winter despite surface freezing.

230 The gauged part of the basin, modelled for this study, is covered by 14 grid cells of the MRB model grid
231 (0.125° x 0.125°) and can thus be hydrologically assessed in terms of the quality of the streamflow
232 simulations. However, this is not the main focus of this study. Parameters for the MESH model are taken
233 from calibrations of the adjacent Liard sub-basin (Elshamy et al., in preparation).



234 The basin and adjacent basins (e.g. Scotty Creek) have been subject to extensive studies as the warm, thin,
235 and sporadic permafrost underling the region has been rapidly degrading (Calmels et al., 2015; Quinton
236 et al., 2011). The region is vulnerable to permafrost thaw, which is changing the landscape of the region,
237 the vegetation, and wildlife habitat with significant implications for First Nations livelihoods and access to
238 their cultural resources. Collapse of forested peat plateaux into wetland areas has been reported by
239 several researchers (e.g. Calmels et al., 2015; Quinton and Baltzer, 2013)

240 Several permafrost-monitoring sites have been established in and around the basin mostly as part of the
241 Norman Wells to Zama pipeline monitoring program launched by the Government of Canada and Enbridge
242 Pipeline Inc. in 1984-1985 to investigate the impact of the pipeline on the permafrost and terrain
243 conditions (Smith et al., 2004). The details of those sites are given in Table 1 while Figure 4 shows their
244 locations. We focus on sites 85-12A and 85-12B as representative of the basin. We use Cables T4 at each
245 site as they are the least affected by the pipeline, being out of its right of way (at least 20m away). Site
246 85-12A has no permafrost while site 85-12B, in close proximity, has a thin (3-4m) permafrost layer with
247 ALD of about 1.5m as estimated from soil temperature envelopes over the period 1986-2000. All other
248 monitoring points on Figure 4 have no permafrost conditions since their records began in the 1980s and
249 1990s. The sites 85-12A & B have a ground moraine landform with open black spruce, ericaceous shrubs,
250 moss-lichen woodland on a peat plateau (Smith et al., 2004). It is challenging to model two different
251 conditions in such close proximity (within the same model grid cell and having the same vegetation). The
252 difference in permafrost conditions is possibly related to the thickness of the peat as shown in the
253 borehole logs (Smith et al., 2004). Borehole 85-12A-T4 has a little over 1m thick layer of peat while
254 borehole 85-12B-T4 has close to 5m peat providing more insulation that keeps the ground from thawing
255 during summer.

256 **Possible Position of Table 1**

257 *3.2.2 Bosworth Creek (Norman Wells)*

258 Bosworth Creek (BWC) is a small basin (126 km²) on the Eastern/Northern Side of the Mackenzie River
259 (Figure 5) draining to the main Mackenzie river near Norman Wells. Permafrost monitoring activities
260 started in the region in 1984 with the construction of the Norman Wells to Zama buried oil pipeline as
261 mentioned above. The basin is dominated by boreal (deciduous, coniferous and mixed) forest. It is located
262 in the extensive discontinuous permafrost zone with relatively deep active layer (1-3 m) and relatively
263 thick (10-50m) permafrost (Smith and Burgess, 2002)



264 There is an ECCC weather station nearby at Norman Wells with complete temperature and precipitation
265 records from 1980. The Canadian Climate Normals (1981–2010, ECCC) at Norman Wells indicate that the
266 mean annual temperature is -5.1°C with temperatures generally below freezing during October to April
267 while the maximum summer temperature of 17.1°C is reached in July. Mean annual precipitation is about
268 294 mm/year, of which around 60% falls as rain while the rest is snowfall.

269 Similar to the Jean Marie River Basin, the streamflow is dominated by snowmelt with a peak in May and
270 a secondary summer peak in some years. WSC Gauge 10KA007 at the outlet of the basin near its
271 confluence with the Mackenzie River has a good record over the period 1980-2016 with a long gap from
272 1995-2008. The mean annual discharge over the available period of record is $0.67\text{ m}^3/\text{s}$ with peaks ranging
273 normally between 2.5 and $15\text{ m}^3/\text{s}$. The highest daily flow on record reached about $20\text{ m}^3/\text{s}$ in May 1991.
274 There is a visible baseflow component for this basin. The basin covers portions of three grid cells of the
275 MRB grid (Figure 5) and therefore it is not expected to have adequate simulation for streamflow
276 comparisons.

277 **Possible Position of Figure 5**

278 The basin itself has not been the focus of previous hydrological studies, but there are several permafrost
279 studies of Norman Wells, being at the Northern end of the important pipeline. Sapriza-Azuri et al. (2018)
280 used cable T5 at the pump station site (84-1) to investigate the appropriate soil depth and initial conditions
281 for permafrost simulations, which is a pre-cursor for this current study. They recommend a soil depth of
282 a least 20m to ensure that the simulated ZOD is within the soil profile. However, they based their analysis
283 on cable T5, which is within the right of way of the pipeline and is likely to be affected by its
284 construction/operation.

285 There are several thermal monitoring sites within and close to the basin and the adjacent Canyon Creek
286 basin to its south East – Table 1. There are also a few thaw tubes but their records are short and
287 intermittent. We focus on the Norman Wells pump station site (84-1) and for this study we choose cable
288 T4 as it is more likely to reflect the natural permafrost conditions being out of the right of way of the
289 pipeline. It has a continuous record since 1985 (Smith et al., 2004; Duchesne, personal communication,
290 2017).

291 *3.2.3 Havikpak Creek*

292 Havikpak Creek (HPC) is a small arctic research basin (about 15 km^2 in area) located in the Eastern part of
293 the Mackenzie River basin delta, 2km north of the Inuvik Airport ($68^{\circ}18'15''\text{ N}$, $133^{\circ}28'58''\text{ W}$) in the



294 Northwest Territories (NWT) (Figure 6). The basin is dominated by sparse taiga forest and shrubs, has a
295 cold sub-arctic climate and is underlain by thick permafrost (>300m). The basin is characterized by mild
296 slopes and has an elevation ranging between 60-240m (Krogh et al., 2017).

297 **Possible Position of Figure 6**

298 There is an ECCC weather station at nearby Inuvik airport with hourly temperature record from 1980 and
299 daily precipitation record from 1960. The Canadian Climate Normals (1981–2010, ECCC) at Inuvik indicates
300 that the mean annual temperature is -8.2°C with temperatures generally below freezing during October
301 to April while a maximum summer temperature of 14.1°C is reached in July. Mean annual precipitation is
302 about 241 mm/year; close to half of which is rainfall while the rest falls as snow.

303 The streamflow flow of the basin is dominated by snowmelt with no winter streamflow due to the lack of
304 groundwater contribution (deep permafrost), and some smaller summer events. The streamflow at the
305 outlet of the basin has been measured by ECCC WSC gauge 10LC017 since 1995. The mean annual
306 streamflow at the outlet is about 0.07 m³/s with a maximum of 4.65 m³/s reached in the summer of 2000.
307 The summer peak discharge varied greatly between 0.7 and 4.0 m³/s over the period 1995-2017. However,
308 the basin covers portions of only two grid cells of the MRB grid (Figure 6) and therefore is not expected
309 to have adequate simulation for streamflow comparisons.

310 The basin has been subject to several hydrological studies, especially during the Mackenzie GEWEX Study
311 (MAGS). For example, Marsh et al. (2002) studied the water and energy fluxes from HPC for the important
312 1994/95 hydrological year. More recently, Krogh et al. (2017) modelled its hydrological and permafrost
313 conditions using the Cold Regional Hydrological Model (CRHM) (Pomeroy et al., 2007). They integrated a
314 ground freeze/thaw algorithm called XG (Changwei and Gough, 2013) within CRHM to simulate the active
315 layer thickness and the progression of the freeze/thaw front with time but they did not attempt to
316 simulate the temperature envelopes or the depth/temperature of ZOD.

317 In terms of permafrost-related measurements, soil temperature envelopes are available from Inuvik
318 airport forest and bog sites 01TC02 and 01TC03 respectively. Ground temperatures are measured with
319 multi-sensor temperature cables installed in boreholes going down to 10m and 6.5m in depth at 01TC02
320 and 01TC03 respectively and both are equipped with data loggers (Smith et al., 2016). Temperature
321 sensors failed on the bog site (01TC03) in 2010 and the site was replaced by 12TC01 in the same
322 conditions. In addition, there are three thaw tubes at Inuvik Upper Air station (90-TT-16) just to the west
323 of the basin, at HPC (93-TT-02), and at the Inuvik Airport bog site (01-TT-03) measuring the active layer



324 depth and ground settlement (Smith et al., 2009). The land form and vegetation at Inuvik Airport forest
325 site (01TC02) is described as fluted till plain with open black spruce trees while the other site (01TC03) is
326 an open bog between ridges on the fluted till plain with scattered shrubs in an open bog. The HPC thaw
327 tube is located in a back spruce forest (Smith et al., 2009).

3.3 Soil Profile and Organic Soils

328 As mentioned earlier, Sapriza-Azuri et al. (2018) recommended a total soil column depth (D) of no less
329 than 20m to enable reliable simulation of permafrost dynamics considering the uncertainties involved
330 including parameter uncertainty. Their study is relevant because they used the same model used here
331 (MESH/CLASS). They studied several profiles, down to 71.6m depth. Recent applications of other H-LSMs
332 also considered deep soil column depths; e.g. CLM 4.5 used 42.1m (Oleson et al., 2013) and CHANGE (Park
333 et al., 2013) used 30.5m. After a few test trials with D = 20, 25, 30, 40, 50 and 100m at the different sites,
334 we found that the additional computation time when adding more layers to increase D is outweighed by
335 the reliability of the simulations. The reliability criterion used here is that the temperature envelopes meet
336 well within the soil column depth over simulation period (including spinning-up) such that the bottom
337 boundary condition is not disturbing the simulated temperature profiles/envelopes and ALD (Nicolsky et
338 al., 2007). ZOD (refer to Section 3.1) represents a relatively stable condition to assess that (Alexeev et al.,
339 2007). ZOD reached a maximum of 25m at one of the sites in a few years and thus the total depth was
340 increased to 50m in anticipation for possible changes in ZOD with warming. We show that this depth is
341 adequate at the three sites selected in the subsequent sections.

342 The CLASS thermal boundary condition at the bottom of the soil column is either no-flux (i.e. the gradient
343 of the temperature profile should be zero) or a constant geothermal flux. For this study, we considered
344 the no-flux condition, as data for the geothermal flux are not easy to find at the MRB scale. Nicolsky et al.
345 (2007) ignored the geothermal flux in their study over Alaska using CLM with an 80m soil column. Sapriza-
346 Azuri et al. (2018) showed that the difference in temperature at ZOD between the two cases is within the
347 error margin for geothermal temperature measurements for 60% of their simulations at Norman Wells.

348 The total soil column depth is only one factor in the configuration of the soil. The layering is as critical. In
349 the above-mentioned modelling studies, exponentially increasing soil layer thicknesses were used, aiming
350 to reach the required depth with a minimum number of layers. The exponential formulation creates more
351 layers near the surface, which allows the models to capture the strong soil moisture and temperature
352 gradients there and yet have a reasonable number of layers (15-20) to reduce the computational burden.
353 However, for most of the MRB, the observed ALD is in the range of 1-2m from the surface and the



354 exponential formulations increase layer thickness quickly after the first 0.5-1.0m, which reduces the
355 accuracy of the models, especially for transient simulations. Therefore, we adopted two layering schemes
356 that have more layers in the top 2m, and increased the layer thickness at lower depths, to 50m. The first
357 scheme has the first meter divided into 10 layers, the second meter divided into 5 layers and the total soil
358 column has 23 layers. The second scheme has soil thicknesses increasing more gradually to reach 51.24m
359 in 25 layers following a scaled power law. This latter scheme has an advantage that each layer is always
360 thicker than the one above it (except the second layer) which showed improvements in numerical stability
361 for both temperature and moisture calculations. The minimum soil layer thickness is taken as 10cm as
362 advised by Verseghy (2012) for numerical reasons. CLASS uses an explicit forward difference numerical
363 scheme to solve the energy and water budgets, which can have instabilities when layers have the same
364 thickness. Table 2 shows the soil layer thickness and centers (used for plotting temperature
365 profiles/envelopes) for both schemes.

366

Possible Position of Table 2

367 Finally, the discretization of organic soil is considered separately for each basin based on local information
368 together with the gridded SLC v2.2 at 0.125° resolution (Keshav et al., 2019a). The flexibility of the model
369 can be utilized for the selected basins when modelled separately but to take the information back to the
370 whole MRB, one has to rely on more general information that is available basin-wide. As discussed above,
371 CLASS (Verseghy, 2012) originally configured the first layer as fibric (type 1), the second as hemic (type 2)
372 and the rest as sapric (type 3) as soon as the organic soil flag is activated. We modified that to be
373 configurable such that one can have more than one fibric or hemic layer and switch off the organic soils
374 for the lower layers. Typically we use them in the same order as it reflects the natural decomposition
375 process (fibric at the surface, followed by hemic, then sapric) but with the introduction of configurable
376 layer depths, texture, and initial conditions, it is necessary to have organic layers configurable as well.
377 Fully organic soils are activated when the organic content is 30% or more (Soil Classification Working
378 Group, 1998).

379 For JMR, we tested configurations with about 0.6m organic soil (6 layers using SC1 and 5 under SC2) to
380 over 2m of organic soil. The soil is assumed to be uniform below the fully organic layers and the soil texture
381 is taken from the gridded SLC v2.2 mapping for the MRB mentioned above giving 15% SAND and 15% CLAY
382 and an organic content ranging between 48-59% (Figure 3). 4-7m peat depths have been reported in the
383 surrounding region (Quinton et al., 2011) and by borehole data of the specific permafrost monitoring sites
384 (Smith et al., 2004). Therefore, the organic content in the mineral layers below the fully organic layers is



385 set to 50% until bedrock. This is an exception for this basin which can be generalized for the MRB for high
386 organic content (e.g. > 50%) like this region. The organic configurations used are listed in Table 3. SDEP is
387 set to 7m based on gridding the Shangguan et al. (2017) dataset at the 0.125° resolution (Keshav et al.,
388 2019b). As mentioned in Section 3.1, SDEP marks the hydrologically active horizon below which the soil is
389 not permeable and its thermal properties are changed to those of bedrock material. This makes it an
390 important parameter and the sensitivity of the results to it is assessed by perturbing it within a range (5-
391 15m).

392

Possible Position of Table 3

393 For BWC, the organic map (Figure 3) indicated that organic matter ranges between 27-34%. We tested
394 configurations with 0.3 – 0.8m organic layers. A borehole log for 84-1-T4 site (Smith et al., 2004) shows a
395 thin organic silty layer at the top (close to 0.2-0.3m). Sand and clay content below the organic layers are
396 uniformly taken to be 24% and 24% respectively based on the gridded SLC v2.2 as above and the
397 remainder (52%) is assumed to be silt by CLASS. SDEP ranges between 5-12m. Thus, several values within
398 this range have been tested.

399 The organic content indicated by the gridded soil information at HPC is only 18%, which is lower than the
400 30% threshold to activate fully organic soils. However, Quinton and Marsh (1999) used a 0.5m thick
401 organic layer in their conceptual framework developed to characterise runoff generation in the nearby
402 Siksik creek. Krogh et al. (2017) adopted the same depth for their modelling study of HPC. Therefore, we
403 tested configurations with 0.3-0.8m fully organic layers. Below that, soil texture values are taken from the
404 gridded SLC v2.2 to be 24% Sand and 32% Clay. A mineral soil configuration with 18% organic matter for
405 the top few layers has been also tested (denoted “M-org”). SDEP ranges between 8-10m but values
406 ranging between 5-12m have been tested.

3.4 Land Cover Parameterization

407 As noted above, the model parameters for the three selected basins were pre-specified, given the specific
408 aims of this study. The setups use land cover, vegetation, and hydrology parameters from the MRB setup,
409 which is described in Elshamy et al. (in preparation). The land cover data are based on the CCRS 2005
410 dataset (Canada Centre for Remote Sensing (CCRS) et al., 2010) and the calibration differentiates between
411 the Eastern and Western sides of the basin using the Mackenzie River as a divide. HPC and BWC are on
412 the East side of the river while JMR is on the west side and therefore they have different parameters for
413 some GRU types (e.g. Needleleaf Forest). SDEP, soil texture information and initial conditions were taken



414 as described above and adjusted according to model evaluation versus permafrost related observations
415 (ALD, Temperature envelopes) with the aim to develop an initialization and configuration strategy that
416 can be implemented for the larger MRB model.

417 Special land covers within the MESH framework include inland water, which is parameterized such that it
418 remains saturated. Thus, drainage is prohibited from the bottom of the soil column and it is modelled
419 using flat CLASS (no slope) with a large hydraulic conductivity value. Ideally, water should have no
420 limitation on evaporation but being still treated as a porous media within the current version of CLASS,
421 the top layers are not always fully saturated. Additionally, it was initialized to have a positive bottom
422 temperature and therefore, it does not develop permafrost. Wetlands are treated in a similar way
423 (impeded drainage and no slope) but it has grassy vegetation and it takes the soil properties as described
424 above (Section 3.3). It remains close to saturation but, depending on location, can still be underlain by
425 permafrost. Taliks are easier to develop under wetlands this way.

3.5 Climate Forcing

426 MESH requires climate forcing data for seven climatic variables at a sub-daily time step. For this study we
427 used the WFDEI dataset that covers the period 1979-2016 at 3 hourly resolution (Weedon et al., 2014).
428 The dataset was interpolated linearly from its original 0.5° resolution to the MRB model resolution of
429 0.125°. The high resolution forecasts of the Global Environmental Multiscale atmospheric model – GEM
430 (Côté et al., 1998b, 1998a; Yeh et al., 2002), and the Canadian Precipitation Analysis – CaPA (Mahfouf et
431 al., 2007) datasets, often combined as (GEM-CaPA), provide the most accurate gridded climatic dataset
432 for Canada. Unfortunately, these datasets are not available prior to 2002 when most of the permafrost
433 observations used for model evaluation are available. Wong et al. (2017) performed an inter-comparison
434 of precipitation estimates from several products against observed station data over Canada and found
435 that CaPA and WFDEI products are in good agreement with station observations.

3.6 Spinning up and Stabilization

436 We used the first hydrological year of the climate forcing (Oct 1979-Sep 1980) to spin up the model
437 repeatedly for 2000 cycles while monitoring the temperature and moisture (liquid and ice content)
438 profiles at the end of each cycle for stabilization. We checked that the selected year was close to average
439 in terms of temperature and precipitation compared to the WFDEI record (1979-2016). The start of the
440 hydrological year was selected because it is easier to initialize the first cycle at the end of summer when
441 there is no snow cover or frozen soil moisture content. Stabilization is assessed visually using various plots



442 as well as by computing the difference between each cycle and the previous one making sure the absolute
443 difference does not exceed 0.1° for temperature (which is the accuracy of measurement thermostats) and
444 0.01 for moisture for all layers in the profile. The aim is to determine the minimum number of cycles that
445 can be used to inform the MRB model development, as it is computationally very expensive to spin up the
446 whole MRB model for 2000 cycles. We then assessed the impact of running the model for the period 1980-
447 2016 after 50, 100, 200, 500, 1000, and 2000 spin-up cycles (using the first hydrological year) on the ALD,
448 ZOD, and the temperature envelopes at the three sites for selected years depending on the available
449 observations. We focused on temperature changes as we found moisture profiles to stabilize quickly.

4. RESULTS

4.1 Establishing Initial Conditions

450 Figure 7 shows the temperature profiles at the end of spinning cycles for a selected GRU (NL Forest) for
451 the three selected sites using the two suggested soil layering schemes. NL Forest is representative of the
452 vegetation at the selected thermal sites for the three studied basins (except HPC bog site). As expected,
453 the profile changes quickly for the first few cycles then tends to stabilize so that there is no significant
454 change after 100 cycles and sometimes less. Figure 8 shows the temperature of each layer for the same
455 cases as in Figure 7 versus the cycle number to visualize the change patterns between cycles. There are
456 some small oscillations indicating some numerical issues but they do not cause major differences for the
457 simulations. For some cases/layers, the temperature keeps drifting (mostly cooling) for several hundred
458 cycles before stabilizing (if it occurs). We note a few important things:

- 459 • Changes to the temperature of the bottom layer (TBOT) from the initial value are too small to
460 have any significance; this triggered further testing using different initial values and the impact on
461 stabilization were similar as shown in the next sections. We also checked the model behaviour for
462 shallower soil columns and found that the bottom temperature did change with spinning up
463 within a range that decreased as the total soil depth increased.
- 464 • SC2 gives much more stable results than SC1 with faster stabilization and less drifting for all cases
465 indicating the importance of the vertical discretization scheme
- 466 • For layers where the temperature is drifting, the difference between the temperature after 2000
467 and 100 cycles is usually within 1.0 K .

468

Possible Position of Figure 7



469 The temperature gradient from South to North is clear comparing the different sites as well as the impact
470 of the deeper permafrost in the North on the faster stabilization of temperature at HPC. Stabilization takes
471 generally longer for middle layers at JMR than for BWC or HPC. For the three sites, there is a change in
472 the slope of the profile at the depth corresponding to SDEP showing the importance of this parameter for
473 permafrost simulations. This is due to the change in soil thermal and hydraulic properties above and below
474 SDEP as well as the change of the heat transfer mechanism to become purely conductive below SDEP
475 (there is no moisture). Above SDEP, there is some role for convective heat transfer depending on the
476 moisture content and state (frozen/unfrozen) which in turn depend on soil properties and organic
477 content.

478 **Possible Position of Figure 8**

479 Given the above findings, the remainder of the results focus on SC2 only. Additionally, we considered
480 different values for the bottom temperature based on site location and extrapolation of observed
481 temperature profiles as it cannot be established through spinning-up. Ground temperature
482 measurements rarely go deeper than 20m and thus we do not know whether they are changing or not.
483 There are established strong correlations between near surface ground temperature and air temperature
484 at the annual scale (e.g. Smith and Burgess, 2000) but the near surface ground temperature is taken just
485 a few centimeters below the surface. We spin up the model at the three sites for 2000 cycles for a few
486 cases and then use the initial conditions after a selected number of cycles to run a simulation for the
487 period of record (1979-2016) and assess the differences for ALD, ZOD, and temperature profiles for
488 selected years within that period. The sensitivity of the results to SDEP, TBOT, and the organic
489 content/configuration will then be assessed using 100 spin cycles only.

4.2 Impact of Spinning up

490 Figure 9, Figure 10 and Figure 11 show the simulated ALD, ZOD and temperature envelopes (selected
491 years) at the three study sites respectively using initial conditions after 50, 100, 200, 500, 1000, and 2000
492 spin-up cycles using SC2 and the stated configuration for SDEP, TBOT, and ORG. Most differences are
493 negligible and it is not easy to distinguish the different lines on those figures except for JMR where there
494 are some larger differences in ALD and ZOD for some years depending on the initial conditions used.
495 Assuming that more spinning up get us closer to the correct values, and thus considering the results
496 initiated after 2000 cycles as a benchmark, one can accept an error of a few centimeters in simulated ALD
497 with a smaller number of spin-up cycles. For JMR, this error is about 10% on average, which is much



498 smaller than the error in estimating ALD at this site. We are thus trading computational time for a slight
499 loss of accuracy at some sites, particularly those located in the more challenging sporadic zone.

500 **Possible Position of Figure 9**

501 The figures also include relevant observations to assess the quality of simulations. The simulated ALDs at
502 JMR and HPC are generally over-estimated (Figure 9). For HPC, two configurations are displayed: one with
503 mineral soil that has 18% organic matter for the top 0.6m (denoted M-org), which seems to better
504 represent the conditions at 01TC02; the other has a fully organic soil for the same depth (denoted ORG)
505 which results in a much smaller ALD and is closer to the thaw tube measurements at HPC (93-TT-02). This
506 indicates the large heterogeneity of conditions that can occur in close proximity of each other.
507 Temperature profiles are only shown for the first case as there are no observed temperature at the HPC
508 thaw tube site. For BWC, the ALD simulation is close to the observations for most years but the simulation
509 shows more inter-annual variability while observations show a small upward trend after an initial period
510 of large increase (1988-1992) which may be the result of the disturbance of establishing the site. A couple
511 of observations are marked “extrapolated” as the zero isotherm falls above the first thermistor (located
512 1m deep).

513 **Possible Position of Figure 10**

514 The simulated ZOD (Figure 10) is also over-estimated for JMR while it is close to values deduced from
515 observations for BWC and HPC. In contrast to ALD, observations have larger inter-annual variability than
516 simulation, possibly due to the large spacing of measuring thermistors and the failure of some in some
517 years. For HPC, the fully organic configuration (ORG) is showing more variability than the mineral one (M-
518 org) but both match the depth deduced from observations for 01TC02. In general, matching ZOD to
519 observations is not an objective in itself but its occurrence well within the selected soil depth is more
520 important. The largest value simulated is about 23m for HPC, which is less than half the total soil depth.
521 That indicates that a smaller soil column depth would not be recommended for HPC but could be used for
522 JMR and BWC.

523 **Possible Position of Figure 11**

524 Comparing to the observed envelopes at each site (Figure 11), the simulations look satisfactory in general.
525 The overall shapes of the profiles are captured for JMR and HPC despite the general over estimation of
526 ALD for both sites. At BWC, the active layer depth simulation agrees well with observations but the
527 temperature envelopes are generally colder than observed and gets the minimum envelope gets too cold



528 near the surface. A similar issue happens for JMR. This is not the case for HPC despite it being the coldest
529 site. This turned out to be related to the specification of fully organic soils at JMR and BWC while the
530 envelopes shown for HPC are taken from the mineral configuration that uses 18% organic content. This is
531 discussed further in Section 4.5.

4.3 Impact of Depth to Bedrock (SDEP)

532 SDEP for the above mentioned configurations for each site was perturbed in the range of 5-15m keeping
533 other studied parameters (TBOT and organic configuration) fixed. Figure 12 and Figure 13 show the impact
534 for each site on the average ALD and ZOD over the analysis period (1980-2016) for all land cover types.
535 100 spinning-up cycles were used to initialize those simulations and GRUs vary between the sites. For
536 JMR, wetlands do not develop permafrost while at shallower SDEP values, talik formations (i.e. no
537 permafrost) develop in some years and thus the shown averages on Figure 12 are for those years when
538 the soil is frozen all year round. There is a general tendency for ALD to decrease with deeper SDEP values
539 for all land cover types, especially for fully organic soils (JMR, BWC, and HPC ORG configuration). SDEP has
540 a similar impact on ZOD (Figure 13) for HPC, as the latter seems to decrease with deeper SDEP, but the
541 impact is not the same for BWC and JMR where ALD initially increases/decreases for JMR, BWC
542 respectively then becomes insensitive to SDEP. This possibly depends on the organic configuration. ZOD
543 is generally shallower for JMR followed by BWC and then HPC. Thus, this behaviour might be correlated
544 to the thickness of permafrost that increases in the same order.

545 **Possible Position of Figure 12**

546 **Possible Position of Figure 13**

547 Figure 14 shows how these changes to ALD and ZOD are occurring via changes in the shape of the
548 temperature envelopes. Increasing SDEP actually allows more cooling of the middle soil layers (between
549 0.5 – 10m) which pushes the maximum envelop upwards reducing ALD. The envelopes bend again to reach
550 the specified bottom temperature, which is much clearer for JMR (because it is set to +0.80°C) than BWC
551 and HPC where it is set to a negative value. Differences are larger for HPC for the fully organic soil
552 configuration (ORG) compared to the mineral configuration with 18% organic content (M-org). The
553 straighter envelopes of HPC tend to meet (i.e. at ZOD) at larger depths than the curved ones at BWC and
554 JMR. This cooling effect is possibly related to having moisture in deeper soil layers with deeper SDEP,
555 which affects the thermal properties of the soil as well as induces convective heat transfer.

556 **Possible Position of Figure 14**



4.4 Impact of Bottom Temperature (TBOT)

557 As shown by the spinning-up experiments above, the initial temperature of the deepest layer remains
558 virtually unchanged through the spin-up and thus has to be specified. The bottom of soil column has a
559 zero flux boundary condition (Section 3.3) implying no gradient at the bottom while TBOT is only an initial
560 condition that was expected to converge to a possibly different steady state value at the end of spin-up.
561 Temperature observations as deep as 50m are rare and relationships between that temperature and air
562 or near surface soil temperature are neither available nor appropriate. For the studied sites, it has been
563 estimated from the observed profiles, and perturbed within a range (-3.0 to +1.5°C), which was varied
564 depending on the site condition/location. Figure 15 shows the impact on changing the temperature of the
565 deepest layer on ALD while Figure 16 shows the impact on ZOD. For JMR, increasing TBOT increases ALD
566 quickly so that taliks form under wetlands if $TBOT > 0^{\circ}\text{C}$ and other land cover types follow at higher
567 temperatures such that permafrost does not develop under most canopy types if $TBOT > 1.5^{\circ}\text{C}$. This gives
568 a way to simulate the no permafrost conditions observed at all sites in the basin (except 85-12B-T4). A
569 similar relationship is simulated for BWC as increasing TBOT increases ALD especially for wetlands. ALD at
570 HPC seems little affected by the bottom temperature with either organic configuration because of the
571 generally colder conditions. ZOD is showing low sensitivity to TBOT except for wetlands at JMR.

572 **Possible Position of Figure 15**

573 **Possible Position of Figure 16**

574 Figure 17 shows how the temperature envelopes respond to changes in TBOT. In all cases, the envelopes
575 seem to bend at some depth to try to reach the given bottom temperature. SDEP seems to influence the
576 start of that inflection. This bending towards the given temperature causes another inflection of the
577 maximum envelope closer to the surface. Depending on the depth of that first inflection, ALD may or may
578 not be affected. ZOD is not affected as much but the temperature at ZOD depends on TBOT. There is a
579 noticeable difference at HPC between the fully organic configuration (ORG) and the mineral configuration
580 that has 18% organic content (M-org) with the same depth (0.6m).

581 **Possible Position of Figure 17**

4.5 Impact of Organic Depth (ORG) and Configuration

582 It is believed that organic soils provide insulation to the impacts of the atmosphere on the soil
583 temperature, which would lead to a thinner active layer than the case of a fully mineral soil. This
584 assumption has been tested for the three sites by changing the depth of the fully organic layers (for JMR



585 and BWC) as well as against a mineral soil with relatively high organic content at HPC. The results are
586 sometimes counter-intuitive. Peat plateaux are widespread in the JMR region and thus the fully organic
587 layers are followed by layers of high organic content (50%) till SDEP. Increasing the fully organic layers
588 initially reduces ALD (Figure 18 top) as expected but also reduces ZOD (Figure 18 bottom) quickly. Then
589 the ALD (which is defined mainly by the maximum temperature envelop) increases again which means
590 that more fully organic layers provides less insulation than mineral layers with high organic content. The
591 reason may be related to the larger moisture holding capacity provided by fully organic layers or because
592 the sand content is small and thus the hydraulic conductivity of the mineral layers is low. HPC shows a
593 similar behaviour where 3 organic layers have a similar effect on ALD as 6 layers and the minimum ALD is
594 reached by 4-5 layers. BWC has a different behaviour than the other two sites as ALD increases initially
595 when increasing the fully organic layers from 3 to 4 then decreases gradually. ZOD seems to decrease with
596 increasing the organic depth for most land cover types at the three sites. Wetlands behave in a different
597 way compared to other land cover types at the different sites because it is configured to remain close to
598 saturation as much as possible. At JMR, wetlands are not underlain by permafrost for all organic
599 configurations, which agrees with the literature.

600

Possible Position of Figure 18

601 Figure 19 shows the response of the temperature envelopes to changes in the organic depth. Increasing
602 the organic depth causes much larger negative temperatures near the surface for the minimum envelope
603 but causes the inflection of the minimum envelop to occur at slightly higher temperatures. A similar effect
604 can be seen for the maximum envelop. The maximum envelopes for the different organic depth intersect,
605 which corroborates with the above for ALD. Another interesting feature can be observed comparing the
606 ORG and M-org configurations for HPC in Figure 14 and Figure 17. The M-org configuration has a much
607 smaller temperature range near the surface than the fully organic soil and causes less cooling in the
608 intermediate soil layers (above SDEP) such that the observed profiles are better matched for this site.
609 These results emphasize the need to investigate the soil hydraulic and thermal properties for each case
610 to better understand the role of organic matter and fully organic layers on the moisture and temperature
611 simulations.

612

Possible Position of Figure 19



5. Discussion and Conclusions

613 Permafrost is an important feature of cold regions, such as the Mackenzie River Basin, and needs to be
614 properly represented in land surface hydrological models, especially under the unprecedented climate
615 warming trends that have been observed. The current generation of LSMs are being improved to simulate
616 permafrost dynamics by allowing deeper soil profiles than typically used and incorporating organic soils
617 explicitly. Deeper soil profiles have larger hydraulic and thermal memories that require more effort to
618 initialize. We followed the recommendations of previous studies to select the total soil column depth to
619 be around 50m. The temperature envelopes meet well within the 50m soil column over the simulation
620 period (including spinning-up), i.e. the bottom boundary condition is not disturbing the simulated
621 temperature profiles/envelopes and ALD.

622 We analysed the conventional layering schemes used by other LSMs, which tend to use an exponential
623 formulation to maximize the number of layers near the surface and minimize the total number of layers.
624 We found that the exponential formulation is not adequate to capture the dynamics of the active layer
625 depth and thus tested two other alternative schemes that have smaller thicknesses for the first 2 meters,
626 instead of the conventional exponentially increasing thicknesses. The first scheme (SC1) had equally-sized
627 layers in the first 1m, followed by thicker but equally-sized layers in the second 1m. The second scheme
628 (SC2) was formulated to have increasing thicknesses with depth following a scaled power law, which we
629 found to be more suitable for the explicit forward numerical solution used by CLASS.

630 We discussed the common initialization approaches, including spinning up the model repeatedly using a
631 single year or a sequence of years, spinning up the model in a transient condition on long paleo-climatic
632 records, or combining both of these approaches. Paleo-climatic reconstructions are scarce and provide
633 limited information (e.g. mean summer temperature or total annual precipitation), while LSMs typically
634 require a suite of meteorological variables at a high temporal resolution for the whole study domain.
635 These variables can be stochastically generated at the resolution of interest informed by paleo-records.
636 However, such practice is computationally expensive, especially for large domains and also introduces
637 additional uncertainties. The approach of spinning-up using available 20th century data has been criticized
638 as picking up the anthropogenic climate warming signal that started around 1850 and thus would yield
639 initial conditions that are not representative. However, paleo climatic records also show that the climate
640 has always been transient and there may not exist a long enough period of quasi-equilibrium to start the
641 spinning-up process (Razavi et al., 2015). Spinning-up using a sequence of years is thus more prone to
642 having a trend than a single year and de-trending the sequence is not free of assumptions either.



643 Given the above complications, we investigated the impact of the simplest approach, which is spinning-
644 up using a single year, on several permafrost metrics (active layer depth – ALD, zero oscillation depth
645 where the temperature envelopes meet – ZOD, and annual temperature envelopes). The aim was to
646 determine the minimum number of spinning-up cycles to have satisfactory performance (if reached) and
647 to know how much accuracy is lost by not spinning more. We did this for three sites along a south-north
648 transect in the Mackenzie River Valley sampling the different permafrost zones (sporadic, extensive
649 discontinuous and continuous) in order to be able to generalize the findings to the whole MRB domain.
650 Additionally, we investigated the sensitivity of the results to some important parameters such as the
651 depth to bedrock (SDEP), the temperature of the deepest layer (TBOT), and the organic soil configuration
652 (ORG).

653 The results show that temperature profiles at the end of spinning cycles remained virtually unchanged
654 (i.e. reached a quasi steady state) after 50-100 cycles, when benchmarked against the results of 2000
655 cycles. We focused on temperature for this stability analysis, because we found that the soil moisture
656 profiles (both liquid and frozen) stabilize much earlier during spin-up. In some cases, changes in the middle
657 layers occurred after 100 cycles but the influence of that on the simulated envelopes, ALD and ZOD was
658 found to be small to negligible compared to the uncertainty of observations and the scale of our model.
659 We also found that the selection of the layering scheme has an effect on stabilization and our proposed
660 scheme (SC2) with increasing thicknesses with depth reached stability faster and had less drifting.
661 Therefore, the simple single-year spinning approach seems to be sufficient for our purpose using SC2.

662 We also found that the temperature of the deepest soil layer (TBOT) remained virtually unchanged from
663 the specified initial value even after 2000 spinning cycles. Therefore, this temperature has to be specified
664 by the modeller. For the study sites, we extrapolated it from the observed envelopes and studied the
665 effect of perturbing it around the extrapolated value. This perturbation had small impacts on ALD and
666 ZOD except for JMR in the sporadic zone, but it had a significant impact on the shape of the envelopes.

667 Temperature observations going as deep as 50m are rare. Most of the permafrost monitoring sites in the
668 MRB have up to 20m cables and thus we do not know if temperature of deeper soil layers has been
669 changing over time, and if so, by how much. To take the information back to MRB scale, we recommend
670 using a south to north gradient moving from +1.0 in the sporadic zone to -2.0 in the continuous zone and
671 specifying a spatially variable field as an input initial condition. For this study, we considered only the zero-
672 flux boundary condition. It is possible to test whether a non-zero thermal flux boundary condition could



673 resolve this issue. However, available datasets for the geothermal flux are not transient and estimate
674 those fluxes at depths greater than the 50m used and thus the issue may need further investigation.

675 The analyses also demonstrated the importance of the organic soil configuration (i.e. how many layers
676 and their organic sub-types) and depth to bedrock on the simulated temperature profiles and active layer
677 dynamics. In most cases, we found combinations of TBOT, SDEP, and ORG that produced satisfactory
678 simulations but the impact of organic layering seems to require further investigation, as increasing the
679 thickness of organic layers does not always act to reduce ALD or reduce the cooling in the middle soil
680 layers that should result from increased insulation. There is an interplay between the moisture
681 properties/content and thermal properties of organic soils that needs further investigation. Additionally,
682 we cannot represent mixed canopies using CLASS, e.g. trees or shrubs underlain by moss. Moss could be
683 providing additional insulation under those canopies that is not represented.

684 To conclude, we now have an approach to represent permafrost in MESS/CLASS at the MRB that has the
685 following features:

- 686 - Around a 50m deep soil profile with increasing soil thickness with depth
- 687 - Spinning 50-100 cycles of the first year of record to initialize the moisture and temperature
688 profiles
- 689 - TBOT, SDEP, and soil texture parameters are to be specified spatially. We have processed gridded
690 data for SDEP and soil texture (including organic matter) and modified MESH/CLASS to read these
691 by grid. In preparing these fields, we will use the 30% threshold to activate fully organic soils.

692 It was necessary to increase the flexibility of the MESH framework to accommodate these input formats
693 as well as to produce relevant permafrost outputs. However, the model is still deficient in some ways. For
694 example, the explicit forward numerical solution may be limiting our choices for soil layering and the lack
695 of complex canopies, amongst other things, may be affecting our parameterization of MESH. These
696 findings are not specific to MESS/CLASS and could be beneficial for the LSM community. This study also
697 demonstrated a simple and effective way to use small-scale investigations to inform larger scale
698 modelling. The key is to use the same model at both scales.



Acknowledgements

699 This research was undertaken as part of the Changing Cold Region Network, funded by Canada's Natural
700 Science and Engineering Research Council and by the Canada Excellence Research Chair in Water Security
701 at the University of Saskatchewan.

References

702 Alexeev, V. A., Nicolsky, D. J., Romanovsky, V. E. and Lawrence, D. M.: An evaluation of deep soil
703 configurations in the CLM3 for improved representation of permafrost, *Geophys. Res. Lett.*, 34(9),
704 doi:10.1029/2007GL029536, 2007.

705 Arboleda-Obando, P.: Determinando los efectos del cambio climático y del cambio en usos del suelo en la
706 Macro Cuenca Magdalena Cauca utilizando el modelo de suelo-superficie e hidrológico MESH. [online]
707 Available from: <http://bdigital.unal.edu.co/69823/1/1018438123.2018.pdf> (Accessed 18 April 2019),
708 2018.

709 Bahremand, A., Razavi, S., Pietroniro, A., Haghnegahdar, A., Princz, D., Gharari, S., Elshamy, M. and
710 Tesemma, Z.: Application of MESH Land Surface-Hydrology Model to a Large River Basin in Iran Model
711 Prospective works, in Canadian Geophysical Union General Assembly 2018, p. 3, Niagara Falls., 2018.

712 Best, M. J., Pryor, M., Clark, D. B., Rooney, G. G., Essery, R. L. H., Ménard, C. B., Edwards, J. M., Hendry, M.
713 A., Porson, A., Gedney, N., Mercado, L. M., Sitch, S., Blyth, E., Boucher, O., Cox, P. M., Grimmond, C. S. B.
714 and Harding, R. J.: The Joint UK Land Environment Simulator (JULES), model description-Part 1: Energy and
715 water fluxes, *Geosci. Model Dev*, 4, 677–699, doi:10.5194/gmd-4-677-2011, 2011.

716 Burn, C. R. and Nelson, F. E.: Comment on “A projection of severe near-surface permafrost degradation
717 during the 21st century” by David M. Lawrence and Andrew G. Slater, *Geophys. Res. Lett.*, 33(21), L21503,
718 doi:10.1029/2006gl027077, 2006.

719 Calmels, F., Laurent, C., Brown, R., Pivot, F. and Ireland, M.: How Permafrost Thaw May Impact Food
720 Security of Jean Marie River First Nation, NWT, GeoQuebec 2015 Conf. Pap., (September), 2015.

721 Canada Centre for Remote Sensing (CCRS), Nacional para el Conocimiento y Uso de la Biodiversidad
722 (CONABIO), Comisión Nacional Forestal (CONAFOR), Insitute Nacional de Estadística y Geografía (INEGI)
723 and U.S. Geological Survey (USGS): 2005 North American Land Cover at 250 m spatial resolution, [online]
724 Available from: <http://www.cec.org/tools-and-resources/map-files/land-cover-2005>, 2010.



725 Changwei, X. and Gough, W. A.: A Simple Thaw-Freezing Algorithm for a Multi-Layered Soil using the Stefan
726 Equation, *Permafrost Process.*, 24(3), 252–260, doi:10.1002/ppp.1770, 2013.

727 Côté, J., Gravel, S., Méthot, A., Patoine, A., Roch, M., Staniforth, A., Côté, J., Gravel, S., Méthot, A., Patoine,
728 A., Roch, M. and Staniforth, A.: The Operational CMC–MRB Global Environmental Multiscale (GEM)
729 Model. Part I: Design Considerations and Formulation, *Mon. Weather Rev.*, 126(6), 1373–1395,
730 doi:10.1175/1520-0493(1998)126<1373:TOCMGE>2.0.CO;2, 1998a.

731 Côté, J., Desmarais, J.-G., Gravel, S., Méthot, A., Patoine, A., Staniforth, A. and Roch, M.: The Operational
732 CMC – MRB Global Environmental Multiscale (GEM) Model . Part II : Results, *Mon. Weather Rev.*, 126(6),
733 1397–1418, doi:[http://dx.doi.org/10.1175/1520-0493\(1998\)126<1397:TOCMGE>2.0.CO;2](http://dx.doi.org/10.1175/1520-0493(1998)126<1397:TOCMGE>2.0.CO;2), 1998b.

734 DeBeer, C. M., Wheeler, H. S., Carey, S. K. and Chun, K. P.: Recent climatic, cryospheric, and hydrological
735 changes over the interior of western Canada: a review and synthesis, *Hydrol. Earth Syst. Sci.*, 20(4), 1573–
736 1598, doi:10.5194/hess-20-1573-2016, 2016.

737 Durocher, M., Requena, A. I., Burn, D. H. and Pellerin, J.: Analysis of trends in annual streamflow to the
738 Arctic Ocean, *Hydrol. Process.*, 33(7), 1143–1151, doi:10.1002/hyp.13392, 2019.

739 Ednie, M., Wright, J. F. and Duchesne, C.: Establishing initial conditions for transient ground thermal
740 modeling in the Mackenzie Valley: a paleo-climatic reconstruction approach, in *Proceedings of the Ninth*
741 *International Conference on Permafrost*, edited by D. L. Kane and H. K. M., pp. 403–408, Institute of
742 Northern Engineering, University of Alaska Fairbanks, Fairbanks, Alaska., 2008.

743 Haghnegahdar, A., Tolson, B. A., Craig, J. R. and Paya, K. T.: Assessing the performance of a semi-
744 distributed hydrological model under various watershed discretization schemes, *Hydrol. Process.*, 29(18),
745 4018–4031, doi:10.1002/hyp.10550, 2015.

746 Heggibottom, J. A., Dubreuil, M. A. and Harker, P. T.: Permafrost, in *National Atlas of Canada*, p. MCR
747 4177, Natural Resources Canada., 1995.

748 Husain, S. Z., Alavi, N., Bélair, S., Carrera, M., Zhang, S., Fortin, V., Abrahamowicz, M., Gauthier, N., Husain,
749 S. Z., Alavi, N., Bélair, S., Carrera, M., Zhang, S., Fortin, V., Abrahamowicz, M. and Gauthier, N.: The
750 Multibudget Soil, Vegetation, and Snow (SVS) Scheme for Land Surface Parameterization: Offline Warm
751 Season Evaluation, *J. Hydrometeorol.*, 17(8), 2293–2313, doi:10.1175/JHM-D-15-0228.1, 2016.

752 IPCC: *Climate Change 2014 Impacts, Adaptation, and Vulnerability Part B: Regional Aspects*, edited by V.



- 753 R. Barros, C. B. Field, D. J. Dokken, M. D. Mastrandrea, K. J. Mach, T. E. Bilir, M. Chatterjee, K. L. Ebi, Y. O.
754 Estrada, R. C. Genova, B. Girma, E. S. Kissel, A. N. Levy, S. MacCracken, P. R. Mastrandrea, and L. L. White,
755 Cambridge University Press, Cambridge, United Kingdom and New York, NY, USA., 2014.
- 756 Keshav, K., Haghnegahdar, A., Elshamy, M., Gharari, S. and Razavi, S.: Aggregated gridded soil texture
757 dataset for Mackenzie and Nelson-Churchill River Basins, , doi:<https://dx.doi.org/10.20383/101.0154>,
758 2019a.
- 759 Keshav, K., Haghnegahdar, A., Elshamy, M., Gharari, S. and Razavi, S.: Bedrock depth dataset for Nelson-
760 Churchill and Mackenzie River Basin based on bedrock data by Shangguan et al. (2016), ,
761 doi:<https://dx.doi.org/10.20383/101.0152>, 2019b.
- 762 Kouwen, N.: WATFLOOD: a Micro-Computer Based Flood Forecasting System Based on Real-Time Weather
763 Radar, *Can. Water Resour. J.*, 13(1), 62–77, doi:10.4296/cwrj1301062, 1988.
- 764 Kouwen, N., Soulis, E. D., Pietroniro, A., Donald, J. and Harrington, R. A.: Grouped Response Units for
765 Distributed Hydrologic Modeling, *J. Water Resour. Plan. Manag.*, 119(3), 289–305,
766 doi:10.1061/(ASCE)0733-9496(1993)119:3(289), 1993.
- 767 Krogh, S. A., Pomeroy, J. W. and Marsh, P.: Diagnosis of the hydrology of a small Arctic basin at the tundra-
768 taiga transition using a physically based hydrological model, *J. Hydrol.*, 550(May), 685–703,
769 doi:10.1016/j.jhydrol.2017.05.042, 2017.
- 770 Lawrence, D. M. and Slater, A. G.: A projection of severe near-surface permafrost degradation during the
771 21st century, *Geophys. Res. Lett.*, 32(24), L24401, doi:10.1029/2005GL025080, 2005.
- 772 Lawrence, D. M., Slater, A. G., Romanovsky, V. E. and Nicolsky, D. J.: Sensitivity of a model projection of
773 near-surface permafrost degradation to soil column depth and representation of soil organic matter, *J.*
774 *Geophys. Res. Earth Surf.*, 113(2), 1–14, doi:10.1029/2007JF000883, 2008.
- 775 Lawrence, D. M., Slater, A. G. and Swenson, S. C.: Simulation of present-day and future permafrost and
776 seasonally frozen ground conditions in CCSM4, *J. Clim.*, 25(7), 2207–2225, doi:10.1175/JCLI-D-11-00334.1,
777 2012.
- 778 Letts, M. G., Roulet, N. T., Comer, N. T., Skarupa, M. R. and Verseghy, D. L.: Parameterization of Peatland
779 Hydraulic Properties for the Canadian Land Surface Scheme, *ATMOSPHERE-OCEAN*, 38(1),
780 doi:10.1080/07055900.2000.9649643, 2000.



- 781 Luo, Y., Arnold, J., Allen, P. and Chen, X.: Baseflow simulation using SWAT model in an inland river basin
782 in Tianshan Mountains, Northwest China, *Hydrol. Earth Syst. Sci.*, 16(4), 1259–1267, doi:10.5194/hess-16-
783 1259-2012, 2012.
- 784 Mahfouf, J.-F., Brasnett, B. and Gagnon, S.: A Canadian Precipitation Analysis (CaPA) Project: Description
785 and Preliminary Results, *Atmosphere-Ocean*, 45(1), 1–17, doi:10.3137/ao.v450101, 2007.
- 786 Marsh, P., Onclin, C. and Neumann, N.: Water and Energy Fluxes in the Lower Mackenzie Valley, 1994/95,
787 , doi:10.3137/ao.400211, 2002.
- 788 McBean, G., Alekseev, G., Chen, D., Førland, E., Fyfe, J., Groisman, P. Y., King, R., Melling, H., Vose, R. and
789 H. Whitfield, P.: Arctic Climate: Past and Present Lead, in *Impacts of a Warming Arctic: Arctic Climate*
790 *Impact Assessment*, p. 140., 2005.
- 791 Nicolsky, D. J., Romanovsky, V. E., Alexeev, V. A. and Lawrence, D. M.: Improved modeling of permafrost
792 dynamics in a GCM land-surface scheme, *Geophys. Res. Lett.*, 34(8), 2–6, doi:10.1029/2007GL029525,
793 2007.
- 794 Oleson, K. W., Lawrence, D. M., Bonan, G. B., Drewniak, B., Huang, M., Charles, D., Levis, S., Li, F., Riley,
795 W. J., Zachary, M., Swenson, S. C., Thornton, P. E., Bozbiyik, A., Fisher, R., Heald, C. L., Kluzek, E., Lamarque,
796 F., Lawrence, P. J., Leung, L. R., Muszala, S., Ricciuto, D. M. and Sacks, W.: Technical Description of version
797 4.5 of the Community Land Model (CLM) Coordinating., 2013.
- 798 Park, H., Iijima, Y., Yabuki, H., Ohta, T., Walsh, J., Kodama, Y. and Ohata, T.: The application of a coupled
799 hydrological and biogeochemical model (CHANGE) for modeling of energy, water, and CO₂ exchanges
800 over a larch forest in eastern Siberia, *J. Geophys. Res.*, 116(D15), D15102, doi:10.1029/2010JD015386,
801 2011.
- 802 Park, H., Walsh, J., Fedorov, A. N., Sherstiukov, A. B., Iijima, Y. and Ohata, T.: The influence of climate and
803 hydrological variables on opposite anomaly in active-layer thickness between Eurasian and North
804 American watersheds, *Cryosph.*, 7(2), 631–645, doi:10.5194/tc-7-631-2013, 2013.
- 805 Pietroniro, A., Fortin, V., Kouwen, N., Neal, C., Turcotte, R., Davison, B., Versegny, D., Soulis, E. D., Caldwell,
806 R., Evora, N. and Pellerin, P.: Development of the MESH modelling system for hydrological ensemble
807 forecasting of the Laurentian Great Lakes at the regional scale, *Hydrol. Earth Syst. Sci.*, 11(4), 1279–1294,
808 doi:10.5194/hess-11-1279-2007, 2007.



- 809 Pomeroy, J. W., Gray, D. M., Brown, T., Hedstrom, N. R., Quinton, W. L., Granger, R. J. and Carey, S. K.: The
810 cold regions hydrological model: a platform for basing process representation and model structure on
811 physical evidence, *Hydrol. Process.*, 21(19), 2650–2667, doi:10.1002/hyp.6787, 2007.
- 812 Quinton, W. L. and Baltzer, J. L.: Hydrologie de la couche productive d’un plateau tourbeux avec dégel du
813 permafrost (Scotty Creek, Canada), *Hydrogeol. J.*, 21(1), 201–220, doi:10.1007/s10040-012-0935-2, 2013.
- 814 Quinton, W. L. and Marsh, P.: A conceptual framework for runoff generation in a permafrost environment,
815 *Hydrol. Process.*, 13(16), 2563–2581, doi:10.1002/(SICI)1099-1085(199911)13:16<2563::AID-
816 HYP942>3.0.CO;2-D, 1999.
- 817 Quinton, W. L., Hayashi, M. and Chasmer, L. E.: Permafrost-thaw-induced land-cover change in the
818 Canadian subarctic: implications for water resources, *Hydrol. Process.*, 25(1), 152–158,
819 doi:10.1002/hyp.7894, 2011.
- 820 Razavi, S., Elshorbagy, A., Wheeler, H. and Sauchyn, D.: Toward understanding nonstationarity in climate
821 and hydrology through tree ring proxy records, *Water Resour. Res.*, 51(3), 1813–1830,
822 doi:10.1002/2014WR015696, 2015.
- 823 Riseborough, D., Shiklomanov, N., Etzelmüller, B., Gruber, S. and Marchenko, S.: Recent advances in
824 permafrost modelling, *Permafr. Periglac. Process.*, 19(2), 137–156, doi:10.1002/ppp.615, 2008.
- 825 Romanovsky, V. E. and Osterkamp, T. E.: Interannual variations of the thermal regime of the active layer
826 and near-surface permafrost in northern Alaska, *Permafr. Periglac. Process.*, 6(4), 313–335,
827 doi:10.1002/ppp.3430060404, 1995.
- 828 Sapriza-Azuri, G., Gamazo, P., Razavi, S. and Wheeler, H. S.: On the appropriate definition of soil profile
829 configuration and initial conditions for land surface–hydrology models in cold regions, *Hydrol. Earth Syst.*
830 *Sci.*, 22(6), 3295–3309, doi:10.5194/hess-22-3295-2018, 2018.
- 831 Shangguan, W., Hengl, T., Mendes de Jesus, J., Yuan, H. and Dai, Y.: Mapping the global depth to bedrock
832 for land surface modeling, *J. Adv. Model. Earth Syst.*, 9(1), 65–88, doi:10.1002/2016MS000686, 2017.
- 833 Smith, S. L. and Burgess, M.: *Ground Temperature Database for Northern Canada*, 2000.
- 834 Smith, S. L. and Burgess, M. M.: *A digital database of permafrost thickness in Canada.*, 2002.
- 835 Smith, S. L., Burgess, M. M., Riseborough, D., Coultish, T. and Chartrand, J.: *Digital summary database of*
836 *permafrost and thermal conditions - Norman Wells pipeline study sites.*, 2004.



837 Smith, S. L., Ye, S. and Ednie, M.: Enhancement of permafrost monitoring network and collection of
838 baseline environmental data between Fort Good Hope and Norman Wells, Northwest Territories, GSC
839 Curr. Res., 2007.

840 Smith, S. L., Riseborough, D. W., Nixon, F. M., Chartrand, J., Duchesne, C. and Ednie, M.: Data for Geological
841 Survey of Canada Active Layer Monitoring Sites in the Mackenzie Valley, N.W.T., 2009.

842 Smith, S. L., Chartrand, J., Duchesne, C. and Ednie, M.: Report on 2015 field activities and collection of
843 ground thermal and active layer data in the Mackenzie corridor, Northwest Territories, Geol. Surv. Canada
844 Open File 8125, doi:10.4095/292864, 2016.

845 Soil Classification Working Group: The Canadian system of soil classification, third edition, 3rd ed., NRC
846 Research Press, Ottawa, Canada. [online] Available from:
847 http://sis.agr.gc.ca/cansis/publications/manuals/1998-cssc-ed3/cssc3_manual.pdf (Accessed 17 April
848 2019), 1998.

849 Soulis, E. D. E., Snelgrove, K. K. R., Kouwen, N., Seglenieks, F. and Verseghy, D. L. D.: Towards closing the
850 vertical water balance in Canadian atmospheric models: Coupling of the land surface scheme class with
851 the distributed hydrological model watflood, Atmosphere-Ocean, 38(1), 251–269,
852 doi:10.1080/07055900.2000.9649648, 2000.

853 Swenson, S. C., Lawrence, D. M. and Lee, H.: Improved simulation of the terrestrial hydrological cycle in
854 permafrost regions by the Community Land Model, J. Adv. Model. Earth Syst., 4(8), 1–15,
855 doi:10.1029/2012MS000165, 2012.

856 Szeicz, J. M. and MacDonald, G. M.: Dendroclimatic Reconstruction of Summer Temperatures in
857 Northwestern Canada since A.D. 1638 Based on Age-Dependent Modeling, Quat. Res., 44(02), 257–266,
858 doi:10.1006/qres.1995.1070, 1995.

859 Verseghy, D.: CLASS – The Canadian land surface scheme (version 3.6) - technical documentation, Intern.
860 report, Clim. Res. Div. Sci. Technol. Branch, Environ. Canada, (February), 2012.

861 Walvoord, M. A. and Kurylyk, B. L.: Hydrologic Impacts of Thawing Permafrost—A Review, Vadose Zo. J.,
862 15(6), 0, doi:10.2136/vzj2016.01.0010, 2016.

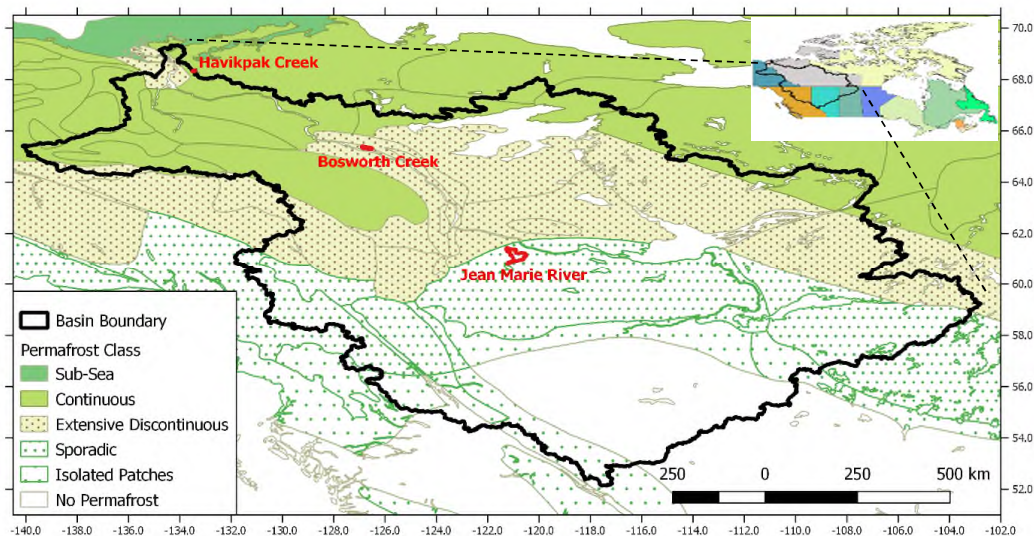
863 Weedon, G. P., Balsamo, G., Bellouin, N., Gomes, S., Best, M. J. and Viterbo, P.: The WFDEI meteorological
864 forcing data set: WATCH Forcing Data methodology applied to ERA-Interim reanalysis data, Water Resour.



- 865 Res., 50, 7505–7514, doi:10.1002/2014WR015638.Received, 2014.
- 866 Wong, J. S., Razavi, S., Bonsal, B. R., Wheeler, H. S. and Asong, Z. E.: Inter-comparison of daily precipitation
867 products for large-scale hydro-climatic applications over Canada, Hydrol. Earth Syst. Sci., 21(4), 2163–
868 2185, doi:10.5194/hess-21-2163-2017, 2017.
- 869 Yassin, F., Razavi, S., Wheeler, H., Sapriza-Azuri, G., Davison, B. and Pietroniro, A.: Enhanced identification
870 of a hydrologic model using streamflow and satellite water storage data: A multicriteria sensitivity analysis
871 and optimization approach, Hydrol. Process., 31(19), 3320–3333, doi:10.1002/hyp.11267, 2017.
- 872 Yassin, F., Razavi, S., Elshamy, M., Davison, B., Sapriza-Azuri, G. and Wheeler, H.: Representation of Water
873 Management in Hydrological and Land Surface Models, Hydrol. Earth Syst. Sci. Discuss., 1–35,
874 doi:10.5194/hess-2019-7, 2019.
- 875 Yeh, K.-S., Côté, J., Gravel, S., Méthot, A., Patoine, A., Roch, M., Staniforth, A., Yeh, K.-S., Côté, J., Gravel,
876 S., Méthot, A., Patoine, A., Roch, M. and Staniforth, A.: The CMC–MRB Global Environmental Multiscale
877 (GEM) Model. Part III: Nonhydrostatic Formulation, Mon. Weather Rev., 130(2), 339–356,
878 doi:10.1175/1520-0493(2002)130<0339:TCMGEM>2.0.CO;2, 2002.
- 879 Zhang, T., Barry, R. G., Knowles, K., Heginbottom, J. A., Brown, J., Zhang, T., Barry, R. G., Knowles, K.,
880 and Heginbottom, J. A.: Polar Geography Statistics and characteristics of permafrost and ground-ice
881 distribution in the Northern Hemisphere, , doi:10.1080/10889370802175895, 2008.
- 882 Zhang, X., Flato, G., Kirchmeier-Young, M., Vincent, L. A., Wan, H., Wang, X., Rong, R., Fyfe, J. C. and L, G.:
883 Changes in Temperature and Precipitation Across Canada, in Canada’s Changing Climate Report, edited
884 by E. Bush and D. S. Lemmen, pp. 112–193, Ottawa, Ontario., 2018.
- 885



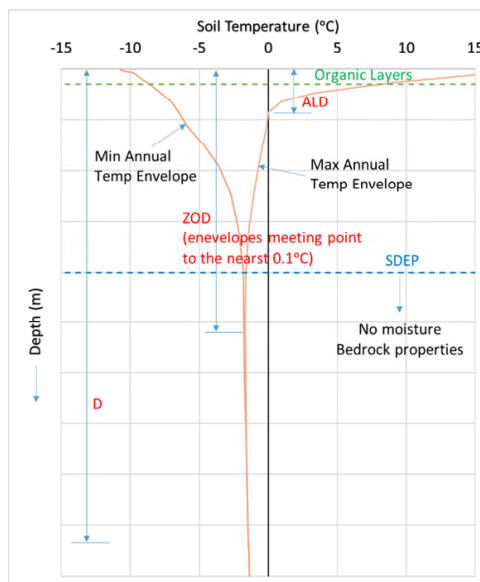
Figures



886

887

Figure 1 Mackenzie River Basin: Location, Permafrost Classification, and the Three Study Sites

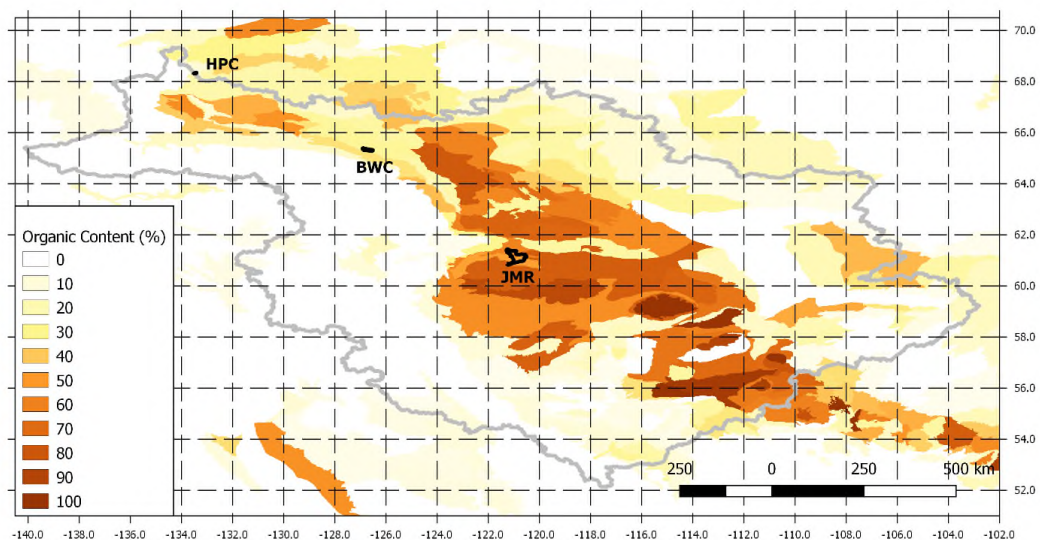


888

889

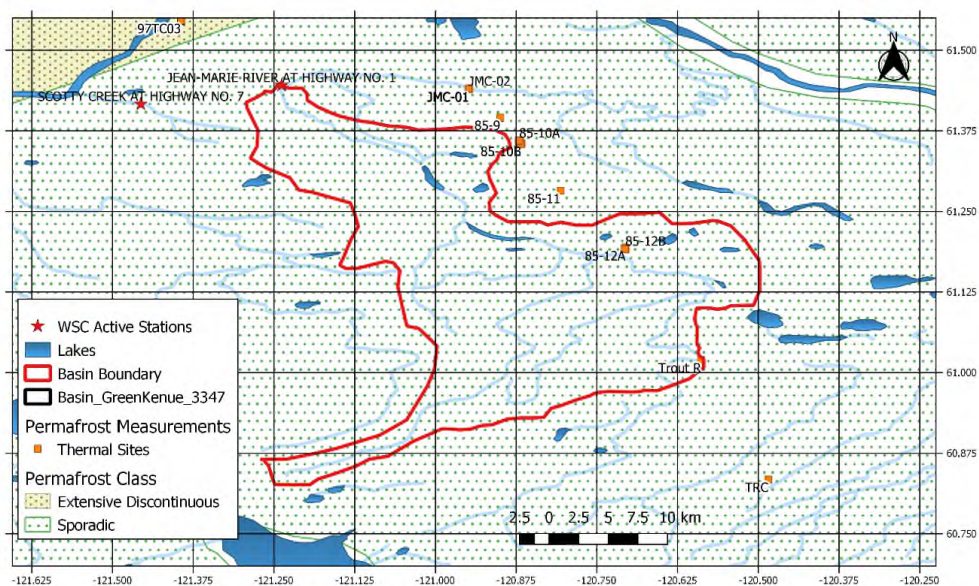
Figure 2 Schematic of the Soil Column showing the Main Variables used to Study Permafrost

890



891

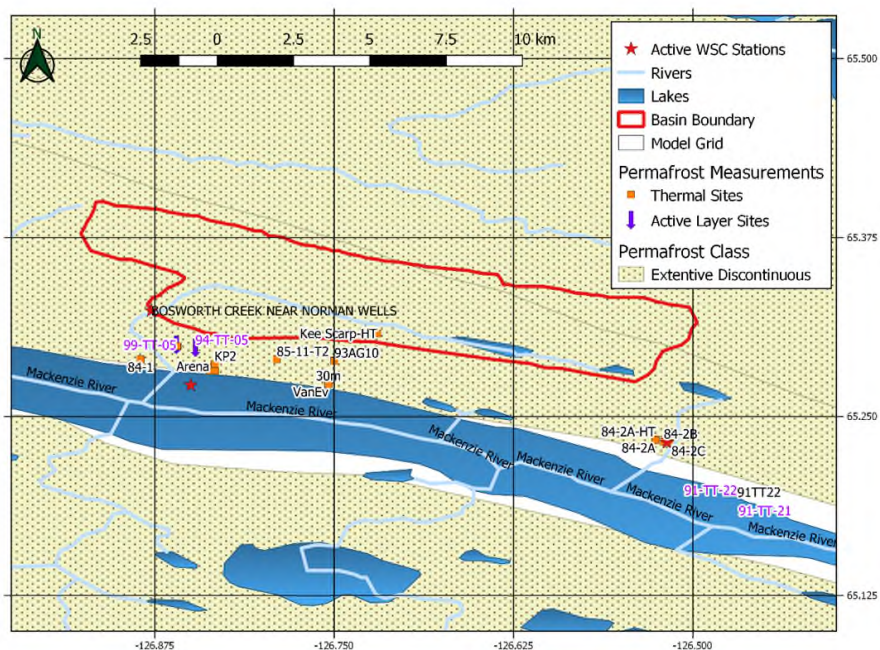
892 *Figure 3 Processed Percentage of Organic Matter in Soil at 0.125° from SLC v2.2 Dataset (Centre for Land*
 893 *and Biological Resources Research, 1996)*



894

895

Figure 4 Permafrost Measurement Sites around Jean Marie River



896

897

Figure 5 Permafrost Measurement Sites around Bosworth Creek



898

899

900

Figure 6 Permafrost Measurement Sites around Havikpak Creek

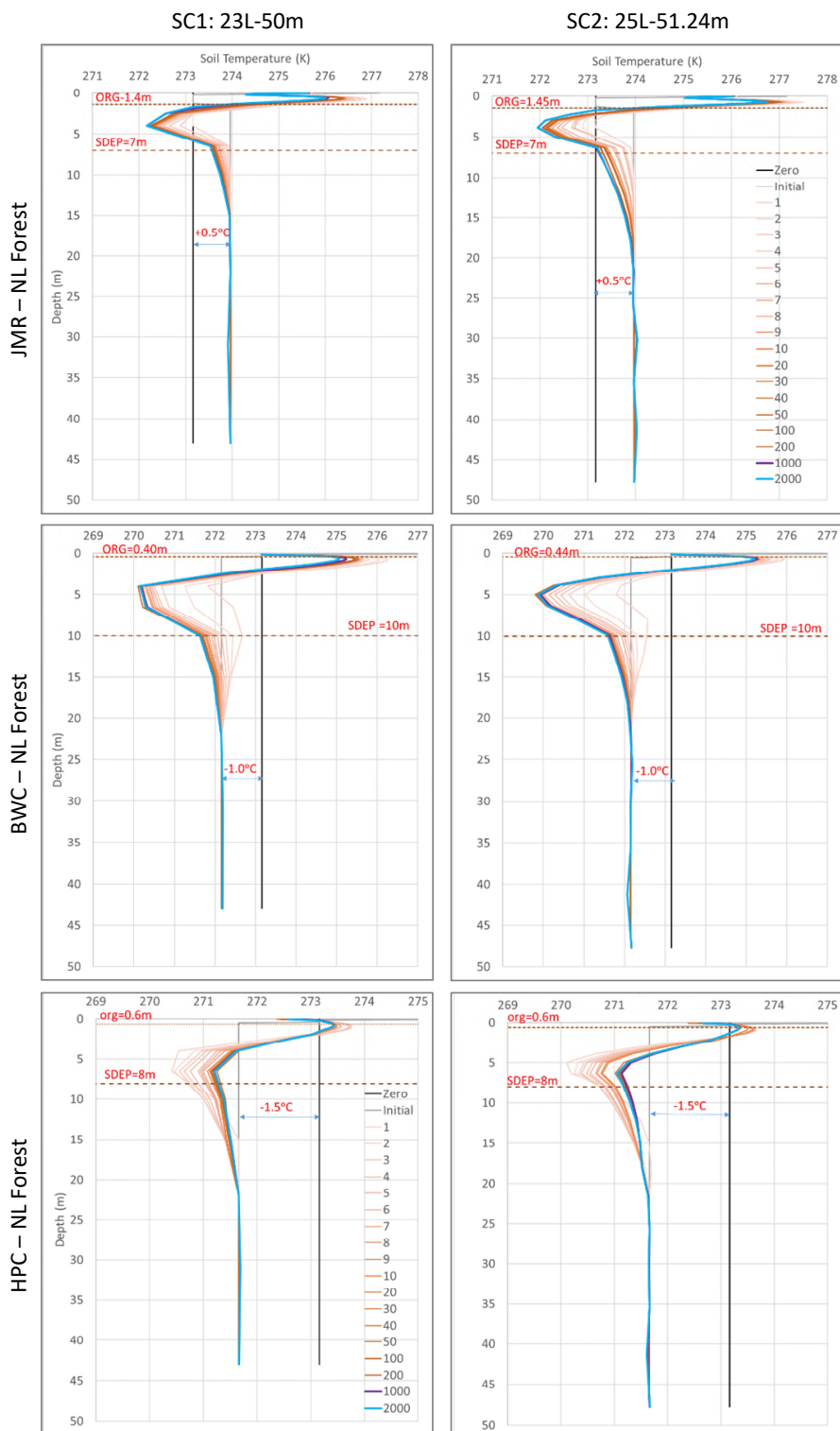




Figure 7 Temperature Profiles at the End of a Range of Spin-up Cycles for NL Forest at the Three Study Sites using Different Soil Layering Schemes

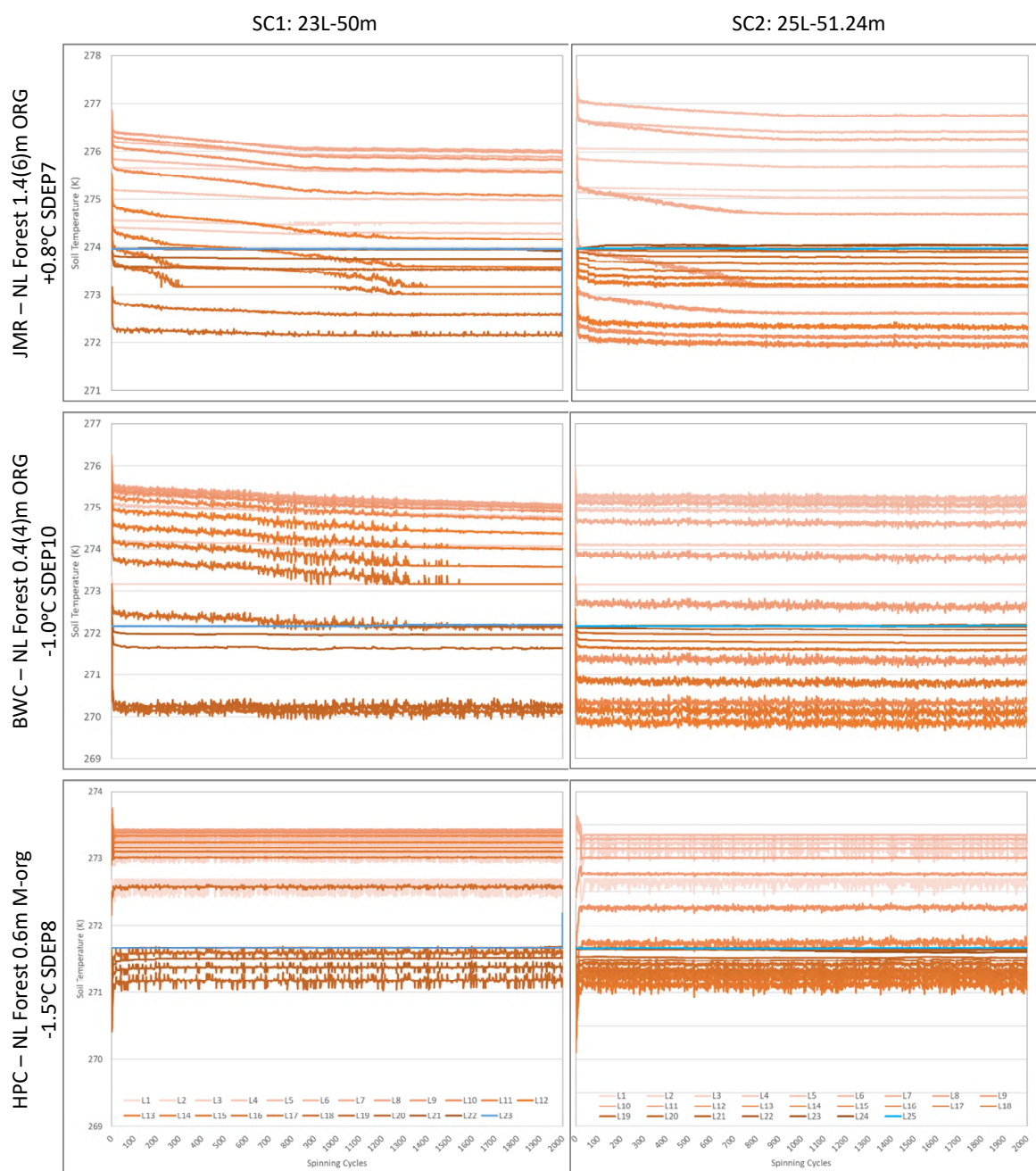


Figure 8 Impact of Soil Layering Scheme Selection on Spin-up Convergence at the Three Study Sites (the darker the color, the deeper the layer, deepest layer is colored blue)

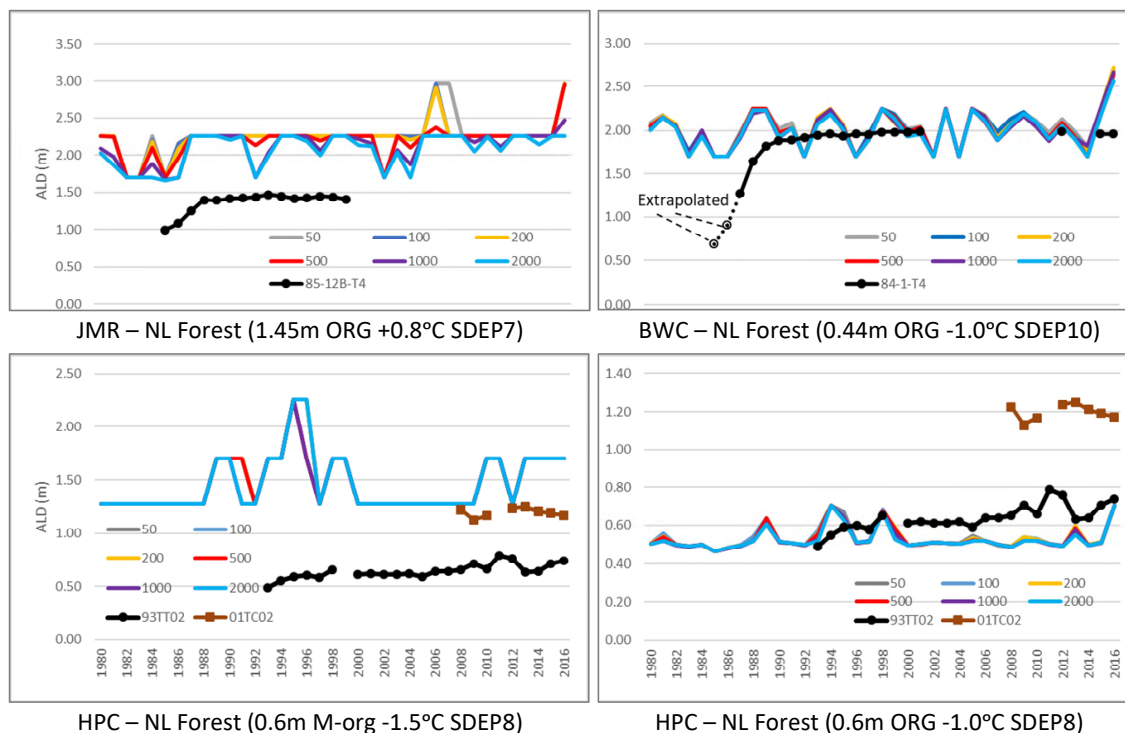


Figure 9 Impact of Number of Spin-up Cycles on Simulated ALD for Needle Leaf Forest Tiles at the Three Study Sites – 2 organic configurations used for HPC

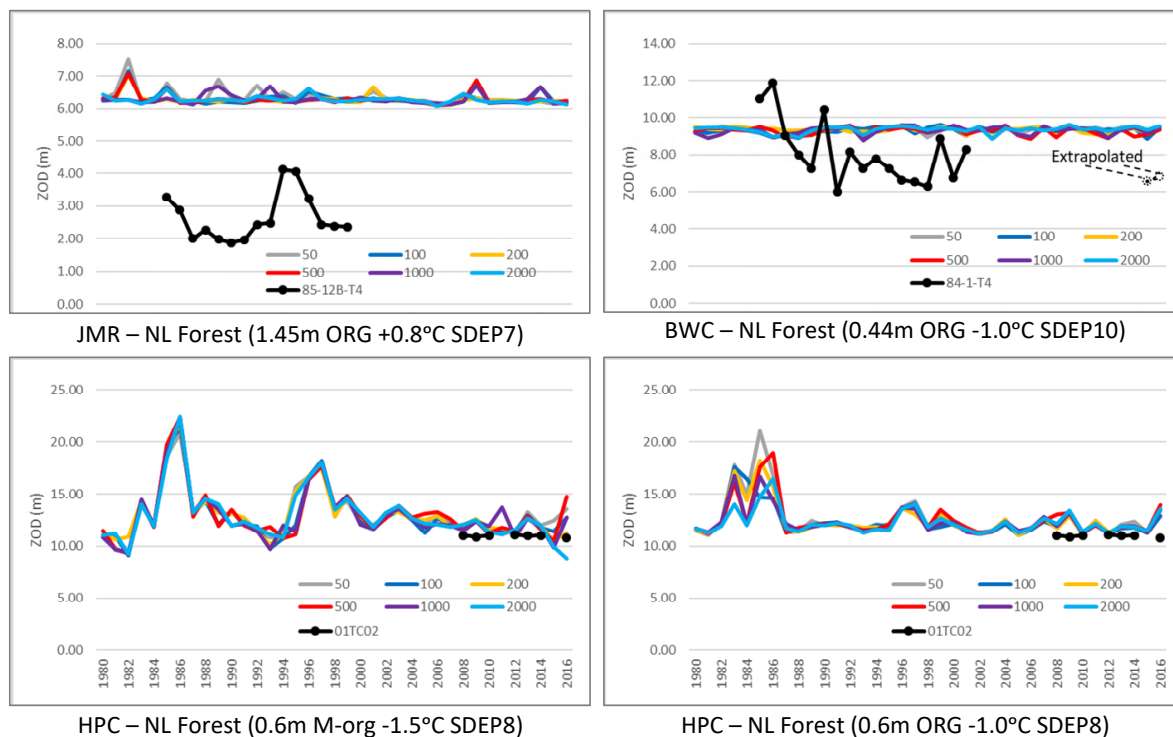


Figure 10 Impact of Number of Spin-up Cycles on Simulated ZOD for Needle Leaf Forest Tiles at the Three Study Sites – 2 organic configurations used for HPC

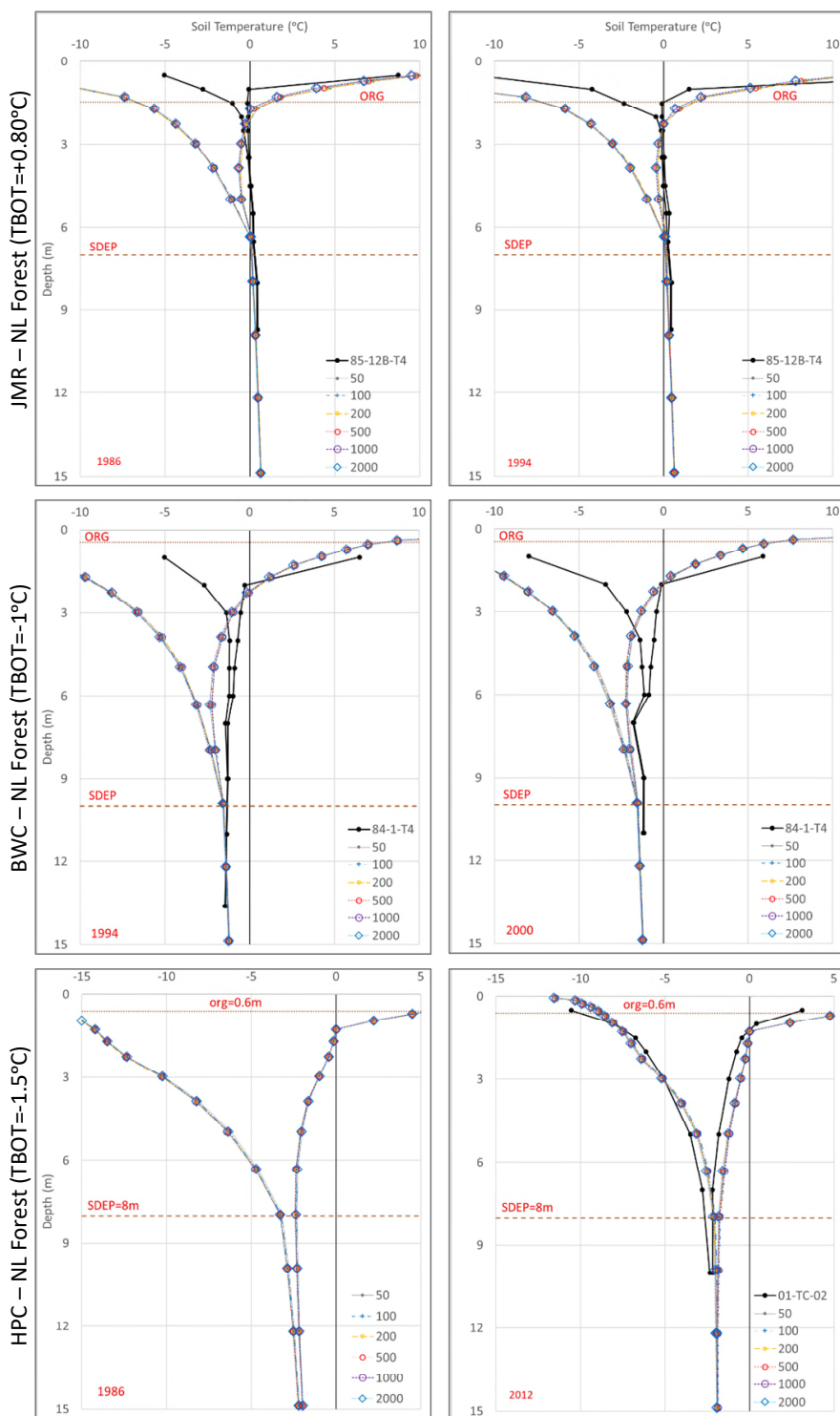


Figure 11 Impact of Number of Spin-up Cycles on Simulated Temperature Envelopes for Needle Leaf Forest Tiles for a Selected Year at Each Study Site (M-org configuration is shown for HPC)

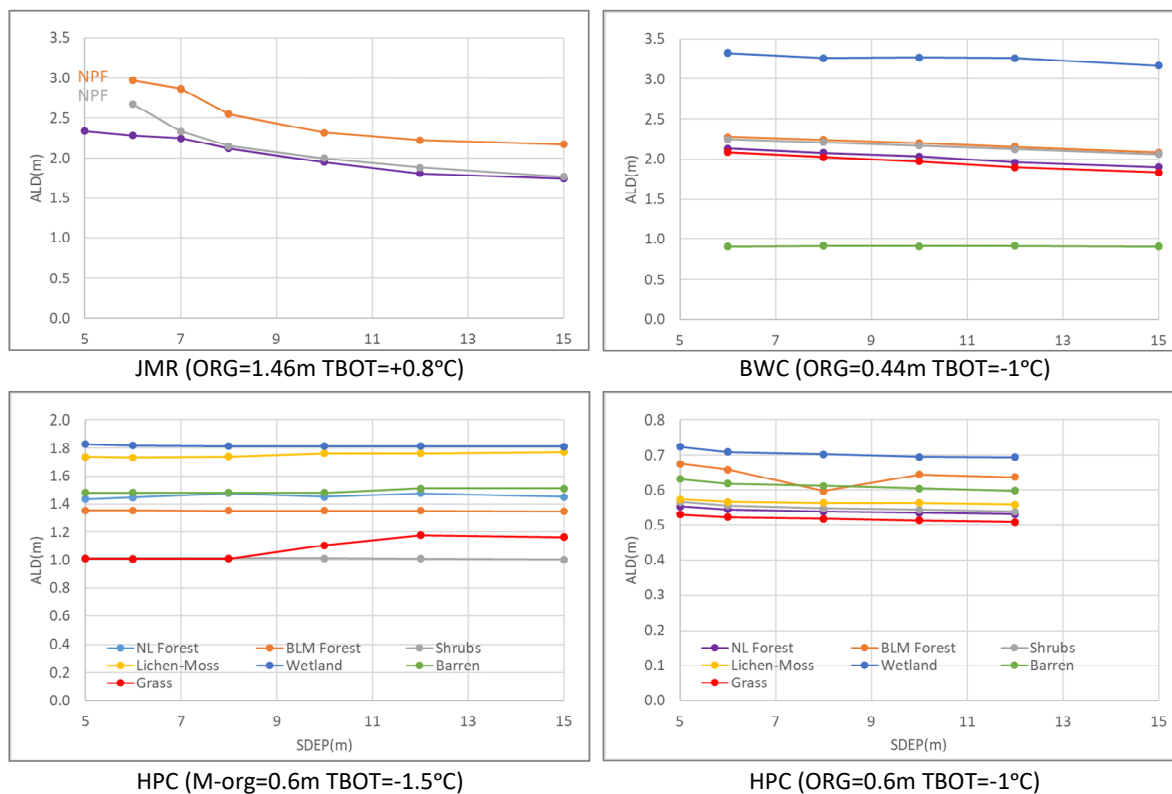


Figure 12 Impact of SDEP on Average Simulated ALD for Different GRUs at the Three Study Sites over the 1980-2016 Period – 2 organic configurations used for HPC

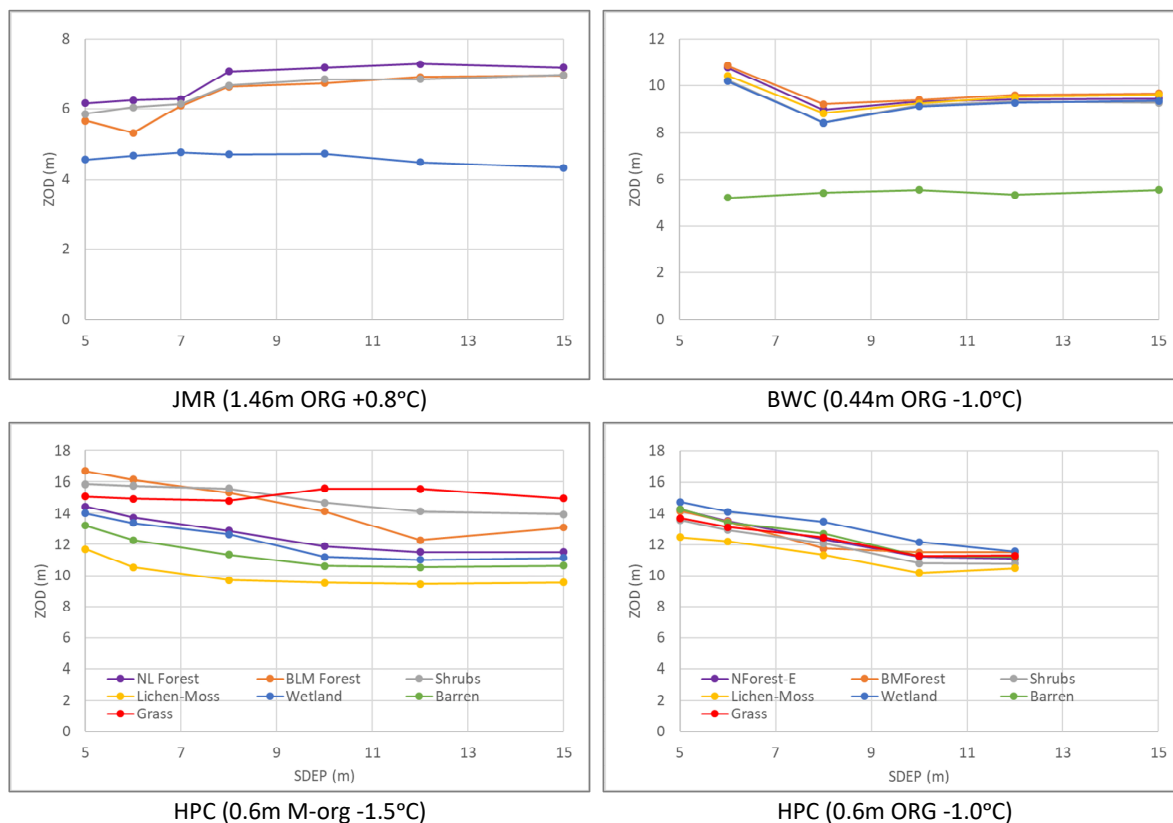


Figure 13 Impact of SDEP on Average Simulated ZOD for Different GRUs at the Three Study Sites over the 1980-2016 Period – 2 organic configurations used for HPC

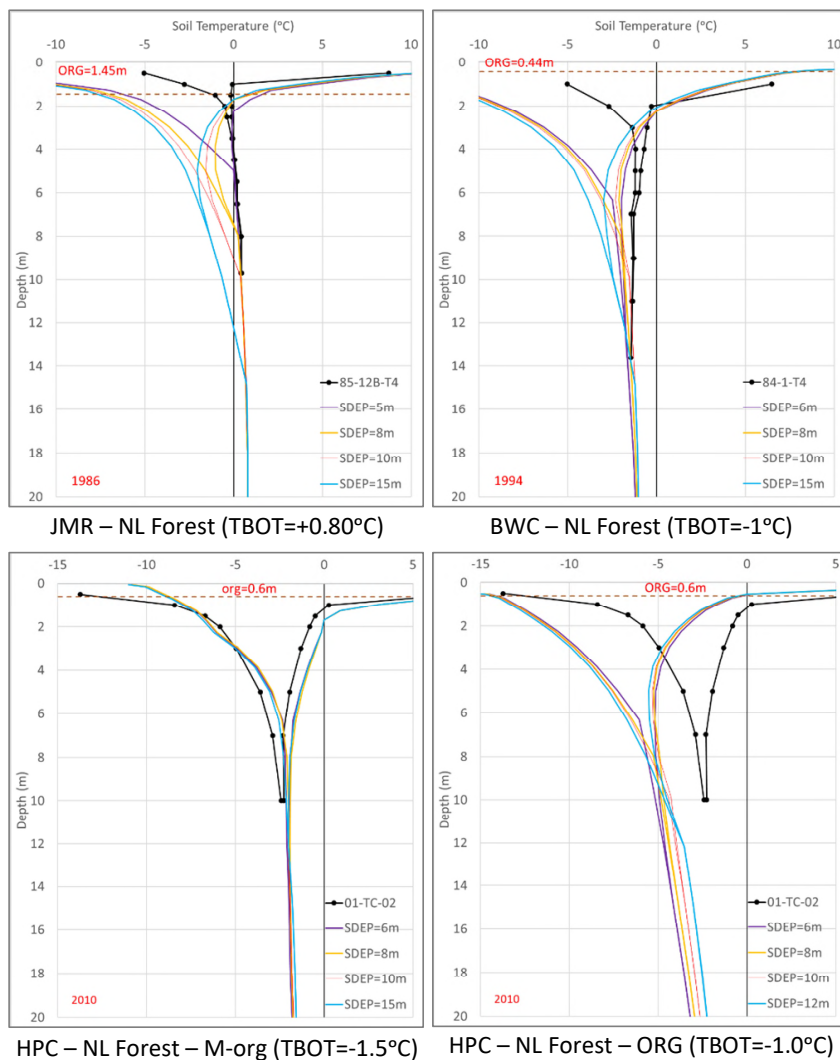


Figure 14 Impact of SDEP on Simulated Temperature Envelopes for Needle Leaf Forest Tiles for a Selected Year at Each Study Site – 2 organic configurations are used for HPC

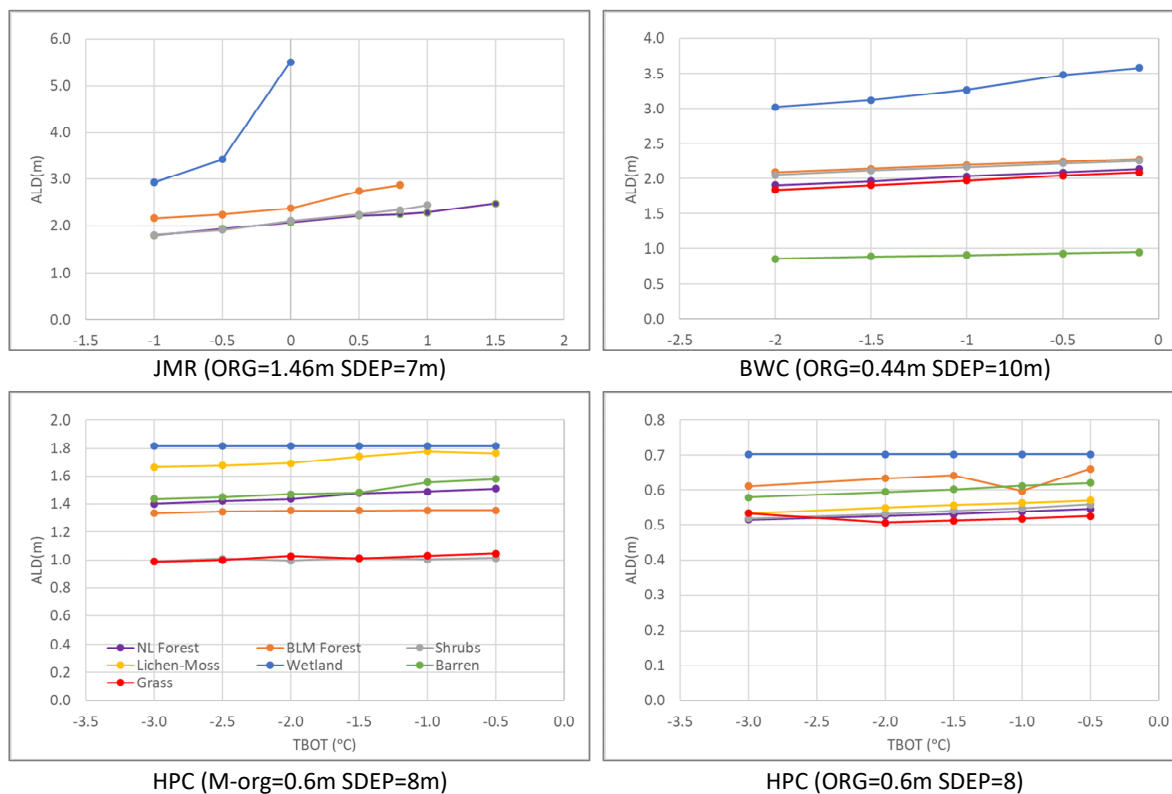


Figure 15 Impact of TBOT on Average Simulated ALD for Different GRUs at the three sites over the 1980-2016 period – 2 organic configurations used for HPC

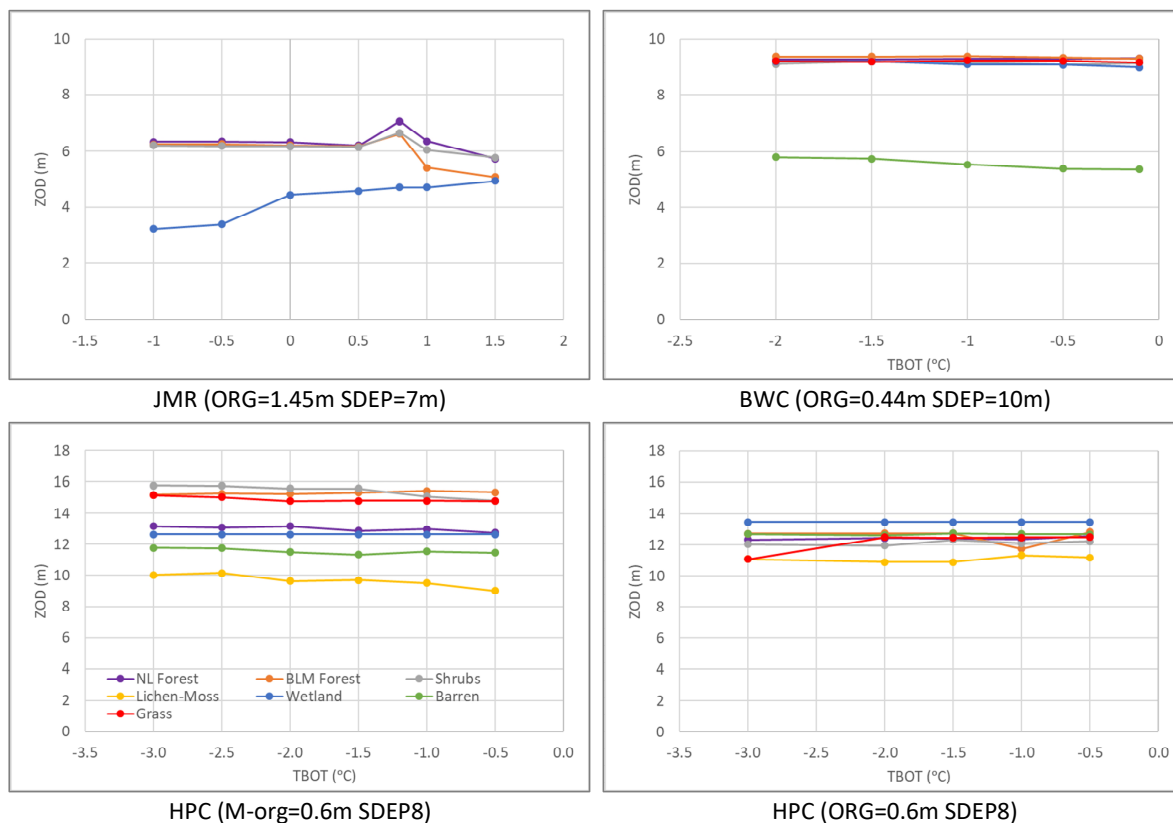


Figure 16 Impact of TBOT on Average Simulated ZOD for Different GRUs at the Three Study Sites over the 1980-2016 Period – 2 organic configurations used for HPC

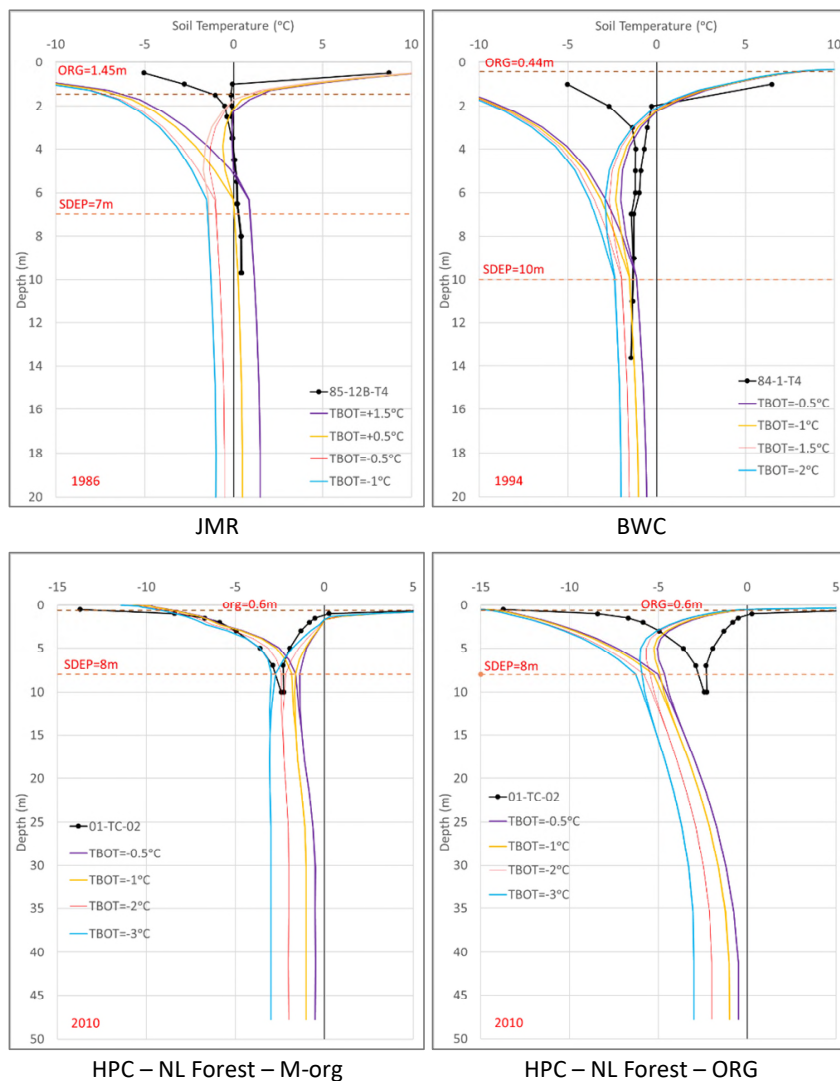


Figure 17 Impact of TBOT on Simulated Temperature Envelopes for Needle Leaf Forest Tiles for a Selected Year at each Study Site – 2 organic configurations are used for HPC

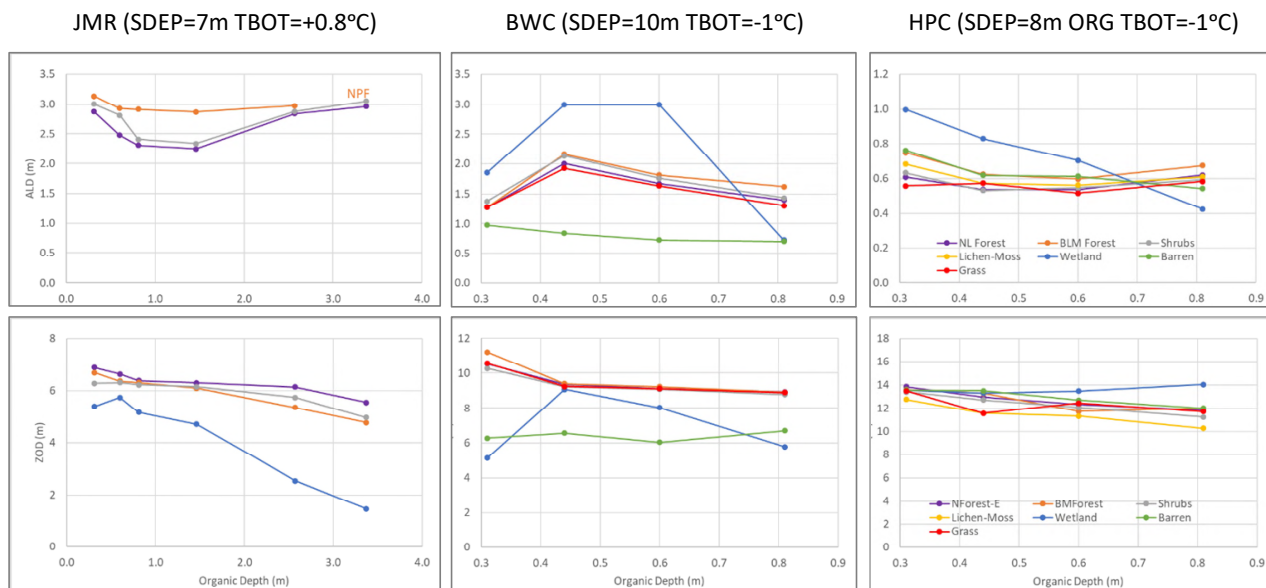


Figure 18 Impact of Organic Depth on Average (1980-2016) Simulated ALD and ZOD for Different GRUs at the Three Study Sites

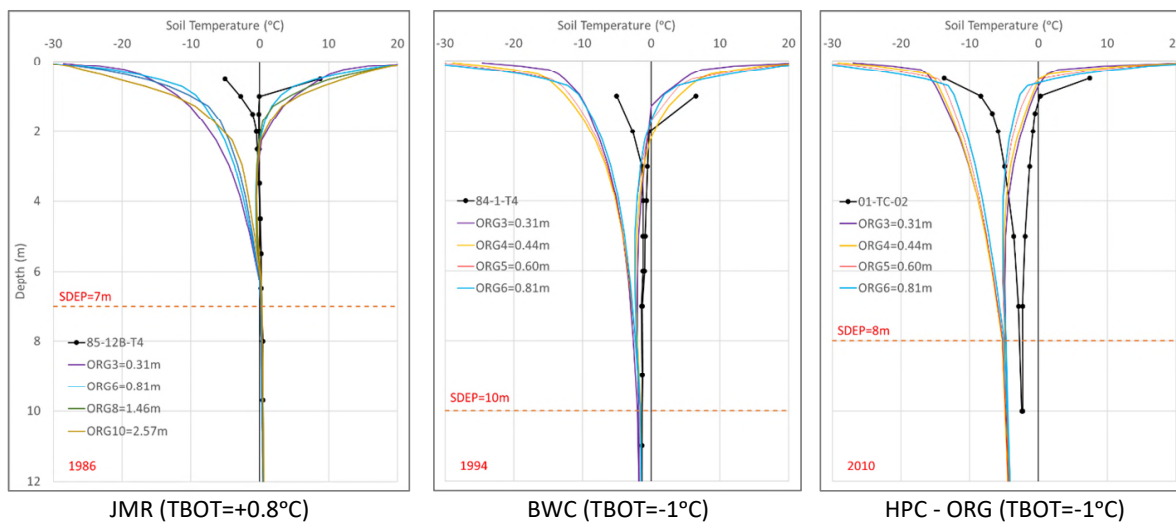


Figure 19 Impact of Organic Soil Depth on Simulated Temperature Envelopes for Needle Leaf Forest Tiles for a Selected Year at Each Study Site



Tables

Table 1 Permafrost Sites and Important Measurements for Study Basins

| Site Name | Site ID | Type | Cables (Depth in m) | Data* | Vegetation | Permafrost Condition |
|---------------------------|----------------|-----------|---|------------------------|--|----------------------|
| JMR (Fort Simpson) | | | | | | |
| Jean-Marie Creek | JMC-01 | Thermal | T1 (5) | 2008-2016 | Shrub Fen | No |
| | JMC-02 | Thermal | T1 (5) | 2008-2016 | Needle Leaf Forest | No |
| Pump Station 3 | 85-9 (NWZ9) | Thermal | T1 (5), T2 (5), T3 (20), T4 (20) | 1986-1995, 2012-2016 | Needle Leaf Forest/Shrubs/Moss | No |
| Jean Marie Creek A | 85-12A | Thermal | T1 (5), T2 (5), T3 (16.4), T4 (12) | 1986-1995 | | No |
| Jean Marie Creek B | 85-12B (NWZ12) | Thermal | T1 (5), T2 (5), T3 (17.2), T4 (9.7) | 1986-2000 | | Yes |
| Mackenzie Hwy S | 85-10A | Thermal | T1 (5), T2 (5), T3 (20), T4 (20) | 1986-1995 | N/A | No |
| | 85-10B | Thermal | T1 (5), T2 (5), T3 (10.5), T4 (10.5) | 1986-1995 | N/A | No |
| Moraine South | 85-11 | Thermal | T1 (5), T2 (5), T3 (12), T4 (12) | 1986-1995, 2014-2016 | N/A | No |
| BWC (Norman Wells) | | | | | | |
| NW Fen | 99-TT-05 | Thaw Tube | | 2009 | Needle Leaf Forest/Moss | Yes |
| | 99-TC-05 | Thermal | Near Surface | 2004-2008 | | |
| Normal Wells Town | Arena | Thermal | T1 (16) | 2014-2015 | Disturbed area adjacent to parking lot | Yes |
| | WTP | Thermal | T1 (30) | 2014-2017 | | Yes |
| KP 2 - Off R.O.W. | 94-TT-05 | Thaw Tube | | 1995-2007 | Needle Leaf Forest/Shrubs/Moss | Yes |
| Norman Wells (Pump Stn 1) | 84-1 | Thermal | T1 (5.1), T2 (5), T3 (10.4), T4 (13.6), T5 (19.6) | 1985-2000 1985-2016 | | Yes |
| Van Everdingen | 30m | Thermal | T1 (30) | 2014-2017 | Needle Leaf /Mixed Forest | Yes |
| Kee Scrap | Kee Scrap-HT | Thermal | T1 (128) | 2015-2017 | Mixed Forest | No |
| HPC (Inuvik) | | | | | | |
| Havikpak Creek | 01-TT-02 | Thaw Tube | | 1993-2017 | Needle Leaf Forest | Yes |
| Inuvik Airport | 01-TT-03 | Thaw Tube | | 2008-2017 | | Yes |
| Inuvik Airport | 90-TT-16 | Thaw Tube | | 2008 | | Yes |
| Upper Air | 01-TT-02 | Thaw Tube | | 2008-2017 | N/A | Yes |
| Inuvik Airport (Trees) | 01-TC-02 | Thermal | T1 (10) | 2008-2017 | Needle Leaf Forest | Yes |
| Inuvik Airport (Bog) | 01-TC-03 | Thermal | T1 (8.35) | | Wetland | Yes |
| | 12-TC-01 | Thermal | T1 (6.5) | 2013-2017 | | Yes |



Table 2 Soil Layering Schemes

| Layer | First Scheme (SC1) | | | Second Scheme (SC2) | | |
|-------|--------------------|--------|--------|---------------------|--------|--------|
| | Thickness | Bottom | Center | Thickness | Bottom | Center |
| 1 | 0.10 | 0.10 | 0.05 | 0.10 | 0.10 | 0.05 |
| 2 | 0.10 | 0.20 | 0.15 | 0.10 | 0.20 | 0.15 |
| 3 | 0.10 | 0.30 | 0.25 | 0.11 | 0.31 | 0.26 |
| 4 | 0.10 | 0.40 | 0.35 | 0.13 | 0.44 | 0.38 |
| 5 | 0.10 | 0.50 | 0.45 | 0.16 | 0.60 | 0.52 |
| 6 | 0.10 | 0.60 | 0.55 | 0.21 | 0.81 | 0.71 |
| 7 | 0.10 | 0.70 | 0.65 | 0.28 | 1.09 | 0.95 |
| 8 | 0.10 | 0.80 | 0.75 | 0.37 | 1.46 | 1.28 |
| 9 | 0.10 | 0.90 | 0.85 | 0.48 | 1.94 | 1.70 |
| 10 | 0.10 | 1.00 | 0.95 | 0.63 | 2.57 | 2.26 |
| 11 | 0.20 | 1.20 | 1.10 | 0.80 | 3.37 | 2.97 |
| 12 | 0.20 | 1.40 | 1.30 | 0.99 | 4.36 | 3.87 |
| 13 | 0.20 | 1.60 | 1.50 | 1.22 | 5.58 | 4.97 |
| 14 | 0.20 | 1.80 | 1.70 | 1.48 | 7.06 | 6.32 |
| 15 | 0.20 | 2.00 | 1.90 | 1.78 | 8.84 | 7.95 |
| 16 | 1.00 | 3.00 | 2.50 | 2.11 | 10.95 | 9.90 |
| 17 | 2.00 | 5.00 | 4.00 | 2.48 | 13.43 | 12.19 |
| 18 | 3.00 | 8.00 | 6.50 | 2.88 | 16.31 | 14.87 |
| 19 | 4.00 | 12.00 | 10.00 | 3.33 | 19.64 | 17.98 |
| 20 | 6.00 | 18.00 | 15.00 | 3.81 | 23.45 | 21.55 |
| 21 | 8.00 | 26.00 | 22.00 | 4.34 | 27.79 | 25.62 |
| 22 | 10.00 | 36.00 | 31.00 | 4.90 | 32.69 | 30.24 |
| 23 | 14.00 | 50.00 | 43.00 | 5.51 | 38.20 | 35.45 |
| 24 | | | | 6.17 | 44.37 | 41.29 |
| 25 | | | | 6.87 | 51.24 | 47.81 |

Table 3 Number of Layers of Each Organic Sub-type for the Organic Configurations Used

| Organic Configuration | Depth (m) | Organic Sub-Type | | |
|-----------------------|-----------|------------------|-----------|------------|
| | | 1 (Fibric) | 2 (Hemic) | 3 (Sapric) |
| 3ORG | 0.31 | 1 | 1 | 1 |
| 4ORG | 0.44 | 1 | 1 | 2 |
| 5ORG | 0.60 | 1 | 2 | 2 |
| 6ORG | 0.81 | 2 | 2 | 2 |
| 8ORG* | 1.46 | 2 | 3 | 3 |
| 10ORG* | 2.57 | 3 | 3 | 4 |
| 11ORG* | 3.37 | 3 | 4 | 4 |

*Only used for JMR